nature neuroscience

Article

https://doi.org/10.1038/s41593-026-02377-y

Representations of the intrinsic value of information in mouse orbitofrontal cortex

Received: 4 November 2024

Accepted: 12 June 2026

Published online: 30 July 2026

Check for updates

Jennifer J. Bussell[1,2] ✉, Ryan P. Badman[3,4], David Márton[3], Ethan S. Bromberg-Martin[5], L. F. Abbott[1,2,6], Kanaka Rajan[3,4] & Richard Axel[1,2,6] ✉

Animals are motivated to seek information that does not influence reward outcomes, suggesting that information has intrinsic value. Here we have developed an odor-based information seeking task that reveals that mice choose to receive information even though it does not alter the reward outcome. Moreover, mice are willing to pay for information by sacrificing water reward, suggesting that information is of intrinsic value to a mouse. We used a microendoscope to reveal neural activity in the orbitofrontal cortex (OFC) while mice learned the information seeking task. We observed the emergence of distinct representations of odors predictive of information and odors predictive of water reward. A latent variable model recapitulated these different representations in the low-dimensional dynamics of OFC neuronal population activity. These data suggest that mice have evolved separate pathways to represent the intrinsic value of information and the extrinsic value of water reward. Thus, the desire to acquire knowledge is observed in mice and the value of this information is represented in the OFC. The mouse now provides a facile experimental system to study the representation of the value of information, a higher cognitive variable.

Humans and other vertebrates exhibit an innate drive to acquire information, even if it does not lead to extrinsic reward. Experiments to understand information seeking have largely involved paradigms in which subjects choose to receive information that reveals but does not alter future uncertain outcomes[1–9]. Subjects are even willing to pay for this information, sacrificing reward for information of no apparent extrinsic value[10–14]. These experiments suggest that the acquisition of information can be of intrinsic value[15,16].

Rewards such as food or water activate physiological pathways that lead to neural representations of reward value[17–19]. Information, however, is a higher-order cognitive variable whose value representations have been more elusive. In functional MRI studies in humans, information seeking tasks elicit a BOLD signal in midbrain and prefrontal reward-associated structures[10,20–25]. Electrophysiological recordings in information seeking paradigms in monkeys have identified a cortex-basal ganglia circuit that extends from the anterior cingulate cortex (ACC) to the lateral habenula, a major regulator of midbrain dopaminergic cells[1,26,27]. Neurons in this pathway respond when reward outcomes are uncertain and diminish their response upon the acquisition of information that eliminates this uncertainty. Moreover, midbrain dopamine neurons respond to stimuli predictive of both information and liquid reward, reflective of prediction error in classical mechanisms of reinforcement[15]. This suggests a circuit in which information activates a cortex-basal ganglia loop, eliciting a dopamine-mediated reward prediction error.

Predicted value is consistently observed in orbitofrontal cortex (OFC) during decision making tasks in both primates and rodents[28–36]. In information seeking tasks, single recorded neurons in monkey

[1]Department of Neuroscience, Columbia University, New York, NY, USA. [2]Zuckerman Mind Brain and Behavior Institute, Columbia University, New York, NY, USA. [3]Department of Neurobiology, Harvard Medical School, Boston, MA, USA. [4]Kempner Institute, Harvard University, Cambridge, MA, USA. [5]Solomon H. Snyder Department of Neuroscience, Johns Hopkins University, Baltimore, MD, USA. [6]Kavli Institute for Brain Science, Columbia University, New York, NY, USA. ✉e-mail: jjb2201@columbia.edu; ra27@columbia.edu

OFC exhibit a preference for either predicted information or external reward, suggesting the presence of distinct representations of intrinsic and extrinsic value[11]. However, the representation of the intrinsic information value predicted by a sensory stimulus in neural populations and the process by which it acquires value through reinforcement in OFC remain unknown. The circuit that allows an organism to recognize that a sensory stimulus predicts information, a cognitive variable, remains elusive.

Here, we have developed a paradigm to ask whether mice value information that resolves the uncertainty of a probabilistic reward outcome but does not offer any apparent extrinsic reward. In this task, mice learn that odor stimuli predict information, and the intrinsic value of information can be quantified by the willingness of mice to pay for information by sacrificing water reward. We have imaged populations of neurons during learning to reveal the emergence of a distinct representation of the intrinsic value of information in OFC. These results imply that the mouse exhibits an innate desire to acquire information, a higher-order cognitive function. Moreover, the value of information and the value of extrinsic reward are encoded by population structures that can be disentangled in the mouse OFC.

Results

Mice value information

We have developed an information seeking task in which water-deprived mice learn to poke their nose into a center port (Fig. 1a). There they receive one of two different odors that direct them either to the left or right side port (forced trials) where they receive a water reward on 25% of the trials. In the side ports, the mice are exposed to one of two different odors followed by a 10 s delay before the receipt of water. In the 'Information' port, one odor accurately predicts the receipt of water, whereas the second odor signals the absence of a water reward. In the other 'No information' port, the mice receive one of a different pair of odors that provide no information as to the outcome of the trial. Whereas the reward probability is equivalent at the two side ports, the Information port differs in that it provides a mouse with information that predicts the reward outcome. One set of odors at the center port predicts information and a different set of odors at the information side port provides information by predicting water reward. Once the mice have learned the structure of the task, a third odor is also offered at the center port allowing a choice between the Information or No information port (choice trials) on one-third of trials, with these free choice trials pseudo-randomly interleaved with forced trials. Mice are trained to perform this task in multiple stages lasting 5–8 weeks (Extended Data Fig. 1a–h). This task derives from those used previously to study information seeking in primates and other species, including in our own recent work[27]. A bias for choice of the Information port would imply that mice seek knowledge of no apparent extrinsic value since this information does not alter the structure of the task or the reward outcome. We have thus developed an experimental paradigm that allows us to discern whether mice seek information and simultaneously examine neural representations of intrinsic and extrinsic value.

When given a choice at the center port between visiting the Information or No information side ports, mice chose the Information port on 78% (mean, 71–83%, 95% confidence interval (CI), $P = 5.20 \times 10^{-6}$, Wilcoxon sign rank) of the free choice trials across several sessions of preference testing (Extended Data Fig. 1j). We did not observe a difference in preference between male and female mice (Extended Data Fig. 1k). We performed reversals of the Information side location for each animal and observed that 71% of initially information-preferring mice maintained their preference for Information despite its new location (Fig. 1b,d and Extended Data Fig. 1i). Across all trials on both sides, 86% of mice preferred the information port (mean preference 67%, $P = 1.65 \times 10^{-6}$, Wilcoxon sign rank; Fig. 1c). We performed a logistic regression to quantify the dependence of choices on side and information (Extended Data Fig. 1l). Eighty-nine percent of mice had positive information choice bias coefficients (information coefficient >0 at $P < 0.05$). However, 90% of these mice also displayed side bias (significant side bias coefficient at $P < 0.05$). We therefore considered that the failure of 14% of mice to alter their choices upon reversal reflected this side bias and these mice were not studied further.

Several additional observations demonstrate that mice learn the structure of the task and the information-predictive meaning of the center port odor cues. First, we considered that the preference to receive information might also cause mice to move more quickly to the Information port than to the No Information side. Indeed, mice entered the Information port faster than they entered the No Information port on both forced and choice trials (mean forced information reaction time 528 ms, mean forced no information 708 ms, $P = 3.6 \times 10^{-270}$, Wilcoxon rank sum; Fig. 1e). They also made fewer errors when choosing the Information port (mean 93% correct on forced information versus 76% correct on forced no information, $P = 1.93 \times 10^{-5}$, sign-rank test; Extended Data Fig. 1m). Consistent with faster reaction times reflecting the preference for information, we observed a correlation between an index of the reaction time difference on free choice trials ((info − no info)/(info + no info)) and the information preference of each animal (Spearman's correlation $r = 0.34$, $P = 0.031$; Extended Data Fig. 1n). Second, we recorded licks at the reward spout and observed that mice began licking as soon as they entered the No information port but withheld licks in the Information port until the informative odors were presented (Fig. 1f). This indicates that mice learn that the Information center port odor predicts the receipt of a side port odor that predicts water reward, whereas the No information center odor predicts no additional reward information at the side port. Two observations suggest that preference for the information port does not reflect a difference in perceived water reward. First, the actual rate of water received per minute did not differ between Information and No information on correct trials (Extended Data Fig. 1o). Second, information preference was not affected by increasing water satiety over the course of each day's training since mice displayed consistent preference between the beginning and end of each training session (Extended Data Fig. 1p). Thus, mice distinguish the two side ports by their information content rather than a perceived difference in water reward.

We observed behaviors following the mouse's choice of a side port that reflect conditioned responses to the water value predicted by each side port odor[5,9]. Following odor A, the cue that predicts water at the Information port (100% reward), animals remained in the port and licked, but following odor B, the cue signaling the absence of water at the Information port (0% reward), the mice did not lick and left the port (Fig. 1g,h and Extended Data Fig. 2a). Following the two odors at the No information port (25% reward), mice remained in the port and licked (Fig. 1g,h and Extended Data Fig. 2a). We considered the possibility that leaving the port may be of value to a mouse and this might contribute to their preference for the Information port. We therefore developed a version of the information seeking task that provided a cue signaling the reward outcome 2 s before it occurred on all trials. In this version of the task, we observed that mice left both the Information and No information side ports on all trials before receiving reward but returned to the port in proportion to their expectation of water reward (Extended Data Fig. 2b–e). Mice also displayed a strong information preference in this version of the task ($N = 10$, 81% mean information choice, $P = 0.010$, Wilcoxon sign rank; Extended Data Fig. 2c). Thus, the choice of information is not driven by a desire to leave the port.

The preference we observe for the Information port presumably reflects the value of information. We therefore asked whether mice were willing to pay for information, a key signature of information value[10–13,37]. We varied the amount of water reward on information trials over blocks of several sessions (Fig. 1i). Mice continued to prefer information even at the expense of diminished water reward, which allowed us to quantify information value as equivalent to an expected value of 4–6 µl of water (Fig. 1j, black).

https://doi.org/10.1038/s41593-026-02377-y

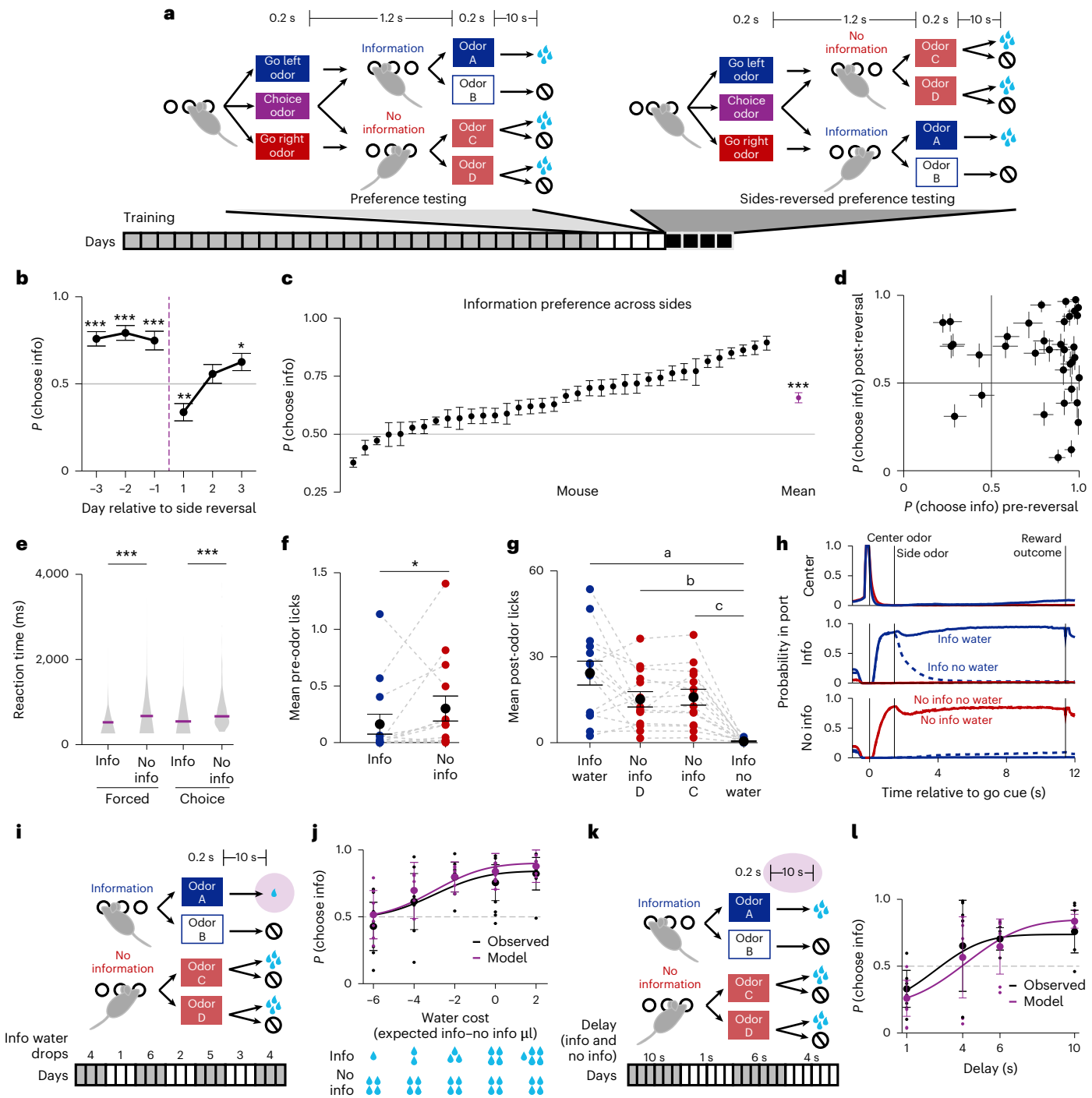

Fig. 1 | Mice value information. a, A schematic of the information choice task. **b**, Information preference around side reversal. The dashed purple line indicates reversal of left–right side identities as in **a**. Mean and 95% CI across animals are shown; two-sided Wilcoxon sign rank, $^{*}P = 0.022$ day 3, $^{**}P = 0.0037$ day 1, $^{***}P = 1.1 \times 10^{-5}$ day −3, $P = 5.9 \times 10^{-6}$ day −2, $P = 8.6 \times 10^{-5}$ day −1, $N = 36$ mice. **c**, Information preference on all choice trials, with information on either side. The black points show binomial choice probability and 95% CIs for each mouse, trial sample sizes listed in Supplementary Table 1. The purple point shows the mean and s.e.m. across animals; $^{***}P = 1.65 \times 10^{-6}$, two-sided sign-rank test, $N = 36$ mice. **d**, Preference for information before and after side reversal. The points show mean information choice probability and 95% CIs in up to the last 200 free choice trials for each animal. **e**, Distribution of reaction times by trial type. Purple indicates the mean; two-sided Wilcoxon rank-sum test, forced $P = 3.6 \times 10^{-270}$, $N = 13{,}787$ trials; choice $P = 9.59 \times 10^{-29}$, $N = 5985$ trials. **f**, Licks at the side ports before odor delivery. The points are for single animals and black shows mean and s.e.m. across animals; two-sided Wilcoxon sign rank test, $P = 0.040$, $N = 14$ mice. **g**, Licks between side odor and water reward delivery. The points are for single animals and black shows mean and s.e.m. across animals, Friedman's ANOVA with Tukey-Cramer correction for multiple comparisons: a, $P = 4.78 \times 10^{-8}$; b, $P = 1.78 \times 10^{-4}$; c, $P = 3.37 \times 10^{-5}$, $N = 14$ mice. **h**, The probability of nose poking in each port by trial type, $N = 36$ mice. **i**, A schematic of information-water value tradeoff sessions. **j**, Information choice probability at different information port water amounts, $N = 4$ mice. Points for single animals; bars, cross-animal mean ±95% CI. Purple, predictions from the RL decision model. **k**, A schematic of sessions manipulating the delay between information and water reward. **l**, The probability of choosing information at different delay durations, $N = 6$ mice. Plot as in **j**.

In our information seeking task, mice move from the center port to a side port where they experience a 10-s delay before receiving a water reward. We expect that if we shorten this delay, the value of information should be reduced because the shortened delay may diminish the duration of the experience of either pleasurable knowledge or aversive uncertainty[2,5,20,38]. We therefore manipulated the value of information by varying the length of delay concurrently on both sides, Information and No information, across blocks of sessions (Fig. 1k). We observed that the preference for information decreased with decreasing delay (Fig. 1l, black).

We developed models to predict choices to receive information across sessions in which we changed the water reward value and delay. We fit a Rescorla–Wagner[39,40] reinforcement learning model to the choices of mice during the water tradeoff and delay tradeoff sessions. The best-fitting model included two separate prediction error value functions, one for water and one for information, that capture the relationship between information preference, information choice history and water reward (equation 9 and Extended Data Fig. 3). We also fit a delay-related discount exponent for the value of information for each animal to quantify the degree to which delay modulates information preference (equation 7). This model fit the choices of all mice in these sessions to ~70–80% accuracy (Fig. 1j,l, red). This decision modeling analysis supports the conclusion that mice compute the value of information separately from the value of water in a manner that is dependent on the duration of the delay between information and reward.

Representations of value in OFC during information seeking

In our behavioral task, different odors predict the intrinsic value of information and the extrinsic value of water reward. In the mouse olfactory system, the identity of an odor is represented in piriform, the primary olfactory cortex, and this representation is largely unaltered when an odor is afforded value[41]. Piriform projects strongly to OFC, which exhibits a neural representation of value only after odor learning[41]. We have therefore asked whether we can detect neural representations of both intrinsic and extrinsic value in OFC as mice perform our information seeking task. If information is of intrinsic value, the center port odors that result in movement to the Information port, whether forced or choice, should serve as conditioned stimuli (CSs) predicting the acquisition of information (Fig. 2a, right). At the Information side port, both odors also provide information. Odor A predicts water reward, whereas odor B predicts its absence. Both odors are therefore unconditioned stimuli (USs) for information. The task also contains analogous CSs and a US for water reward. The Information side port odors predict water reward or its omission and are therefore a CS+ and CS− for water reward. The water reward itself is a US. We have asked whether we can detect representations of these signals of intrinsic information and extrinsic water value in OFC in response to the odors in our task.

We recorded calcium signals reflecting neural activity in 1,138 regions of interest (ROIs) in OFC using miniaturized microscopes in seven mice (Supplementary Table 3 and Extended Data Fig. 4a,b). Neurons in mouse OFC represent task variables including stimulus identity, side choice, confidence, task context and reward value[29–33,42–47]. Moreover, OFC neurons display mixed selectivity: individual cells encode multiple variables and the representations of variables are overlapping[46–50]. Indeed, we observed substantial responses to side location in our recordings. We therefore exploited the reversals of Information side in our task to disambiguate side direction and value encoding. We registered ROI identities in four sessions across the side reversal for each mouse: two with information on the left and two with information on the right (Fig. 2a). We analyzed neural activity from correct forced trials pooled across these sessions, which balanced the number of information and no information trials on each side, following each forced trial odor to control for the potential influence of side and odor identity on neural activity. Individual registered ROIs displayed highly stable odor-evoked activity across sessions[51] (Extended Data Fig. 4c–m) and we refer to them as neurons for simplicity.

We focused on differential activity between information–no information and water reward–no water reward trials to identify representations of information and water value, respectively. We computed coding indices, a cross-validated measure of mean differential activity, to measure individual neuron's encoding of information and water value across the components of the trial (Methods; Fig. 2b).We examined these coding indices across the recorded OFC populations throughout trials in our task (Fig. 2b,c and Extended Data Fig. 5a). We observed an increase in the information coding index across the population following the center port odor, reflecting the information CS ($P < 0.001$, permutation test; Fig. 2c and Extended Data Fig. 5c), and an increase in the information coding index upon exposure to the side port odors reflects the information US ($P < 0.001$, permutation test; Fig. 2c and Extended Data Fig. 5d). We observed an increase in the water coding index following the side port odor across the population, reflecting the water CS ($P < 0.001$, permutation test; Fig. 2c and Extended Data Fig. 5d) and following the receipt of water, reflecting the water US ($P < 0.001$, permutation test; Fig. 2c and Extended Data Fig. 5e). These OFC responses provide neural representations of a CS and US for the intrinsic value of information and a CS and US for the extrinsic value of water reward.

We observed an increased information coding index at the center port reflecting the information CS in 17% of OFC neurons (Fig. 2d and Extended Data Fig. 5b and 6f). Individual cells displayed mixed selectivity and responded to both predicted information and side location[43,48]. Fifty-nine percent of information CS cells also displayed side encoding, with 26% of the total OFC population encoding the side directed by the center port odor (Fig. 2d,e and Extended Data Figs. 5b,c and 6e). Given this mixed selectivity, we sought to define an axis encoding the prediction of information in the high-dimensional space of OFC population activity. We computed the principal components of the difference in activity between information and no information trials balanced across sides. The first principal component captured 80% of the variance in this activity. We then projected each trial's activity onto this first component (Fig. 2f). The separation between projected activity on information versus no information trials illustrates an axis encoding the prediction of information demixed from side and odor identity in response to the center port odor on each trial.

We then used linear classification of data balanced across side reversals to decode information and no information trials (Fig. 2g, left). We were able to decode information versus no information trials at the center port with 73% accuracy ($P = 8.6 \times 10^{-22}$ versus 51% in null distribution) on forced trials and 64% accuracy ($P = 4.9 \times 10^{-19}$ versus 50% in null distribution) on choice trials in pseudo-population data generated across animals (Fig. 2g and Extended Data Fig. 6a). We were also able to decode information versus no information trials from neural activity recorded within individual animals (Fig. 2g and Extended Data Fig. 6b). These classifiers thus define the representation of an information CS in the OFC population that reflects the prediction of information on a trial-by-trial basis in a manner shared across multiple odors predicting information on either the left or right side.

Additional observations confirm that the information CS representation encodes the prediction of information consistently across different sensory stimuli, task contexts and movement responses. First, we observed highly correlated responses to the two different center port odors on forced and choice information trials (Pearson's correlation $r = 0.91$, $P < 1 \times 10^{-308}$; Extended Data Fig. 6c,d,g). Second, the responses we observed to odors predictive of information at the center port do not reflect the animal's movement toward the side port. The increase in the information coding index aligns to the receipt of center port odor rather than the time of leaving the center port or entering the side port (Extended Data Fig. 6h). Moreover, within the population of information prediction-encoding cells, neural activity on a given trial

https://doi.org/10.1038/s41593-026-02377-y

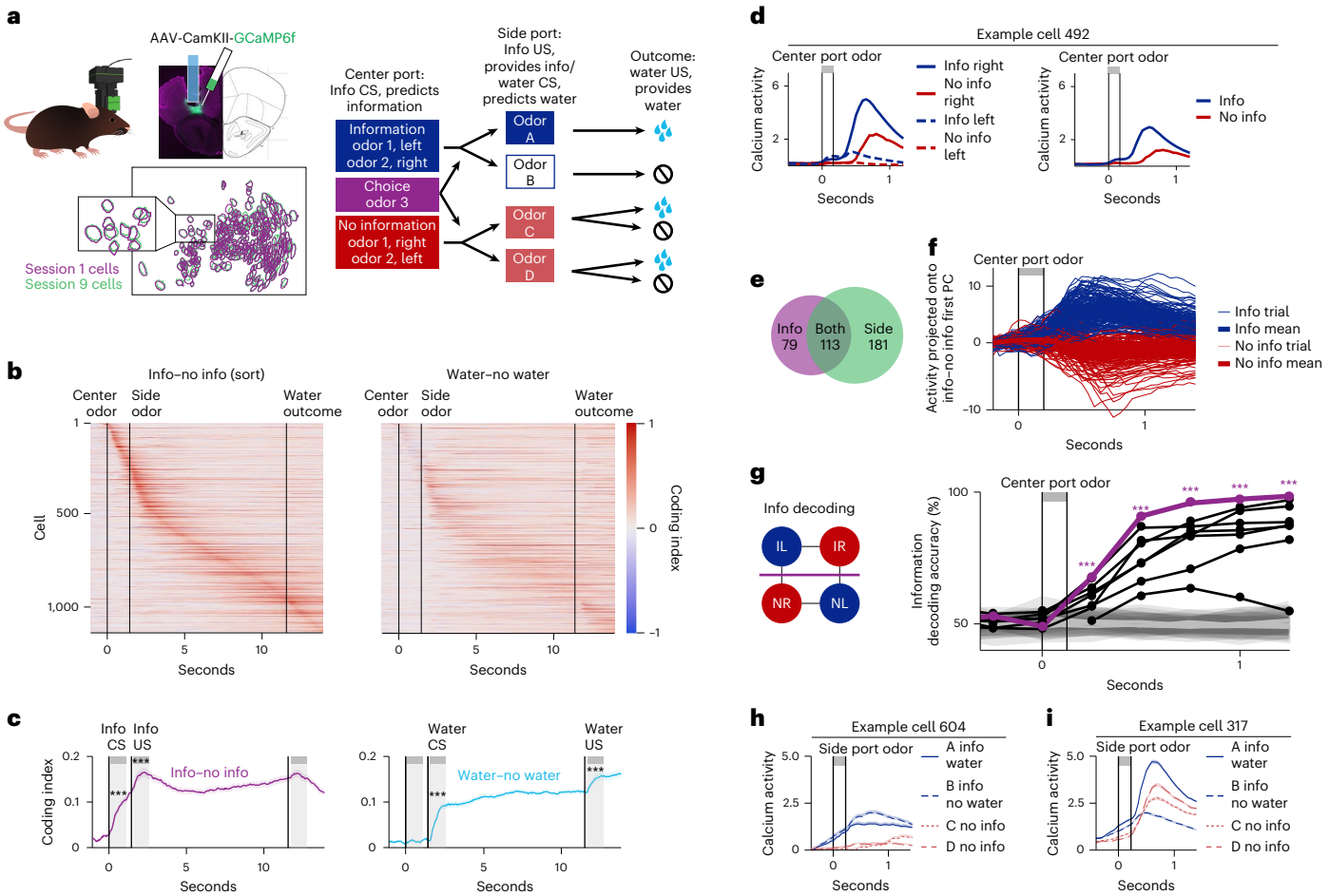

Fig. 2 | Representations of value in OFC during information seeking. **a**, A schematic of imaging technique. **b**, Left: the information coding index across the population. Right: the water coding index. Cells in both were sorted by the information coding index. **c**, Left: population mean information coding index. Right: population mean water coding index. The colored shading shows s.e.m. Gray shading indicates time periods used to identify CS and US value representations by increases in coding index. ***$P < 0.001$, permutation test, trial sample sizes in Supplementary Table 3. **d**, Activity of an example cell at the center port odor. The line shows the mean and shading shows s.e.m. **e**, Overlap between information and side coding cells, $P < 2.00 \times 10^{-30}$, chi-square test, $N = 1{,}138$ cells. **f**, Projection of single trial activity onto the information-encoding axis in the population activity space, $N = 1{,}138$ cells. PC, principal component. **g**, Left: the decoding schematic. IL, info left; IR, info right; NR, no info right; NL, no info left. Right: information versus no information decoding accuracy on forced trials. Purple, pseudo-population with trials sampled across subjects; black, individual animals; gray, shuffled null distributions. ***$P < 0.001$, **$P < 0.01$, *$P < 0.05$, one-sided z score. Exact P values are listed in Supplementary Table 2, $N = 10$ cross-validations. **h**, Activity of an example information US-encoding cell at side port odor. The line shows the mean and shading shows s.e.m. **i**, Activity of an example water CS-encoding cell at side port odor. The line shows the mean and shading shows s.e.m.

is not tightly linked to reaction time, which reflects movement speed (Extended Data Fig. 6i). We therefore conclude that the information CS we describe is a neural representation of predicted information.

The odors A and B provided at the information side port simultaneously serve as an information US and a water CS. Both odors provide information (US), while odor A predicts water reward (CS+) and odor B predicts no water reward (CS−). We observed representations of each of these value signals in individual cells. First, 25% of OFC cells displayed an increased information coding index following the side port odors (Extended Data Fig. 5b), reflecting the information US. Activity following odor A (25% of information trials) was greater than that following odor D (25% of no information trials, $P < 0.001$, permutation test; Extended Data Fig. 6j), and odor B responses (75% of information trials) were greater than those following odor C (75% of no information trials, $P < 0.001$, permutation test; Extended Data Fig. 6j). Moreover, the responses to odors A (water) and B (no water) were highly correlated across cells (Pearson's correlation $r = 0.69$, $P < 0.001$; Extended Data Fig. 6l). Most cells that responded to odor A also responded to odor B, albeit often more weakly (Extended Data Fig. 6j,k). One example cell reflects the shared information US representation of both odors A and B (Fig. 2h). Second, 21% of OFC cells displayed an increased water coding index at the side port, reflecting the differential responses to odor A (water, CS+) and odor B (no water, CS−) that comprise the water CS (Extended Data Fig. 5b). Across the population, this A versus B difference was greater than the differential activity between no information odors C and D observed in 10% of OFC cells (Extended Data Fig. 5b,d). One example water CS-encoding cell responds most to odor A and least to odor B, with intermediate activity following odors C and D (Fig. 2i).

We also observed individual cells whose activity reflected the water US, responding to the receipt of water on both information and no information trials (Extended Data Figs. 5b and 6m,n). These cells responsive to water on the Information and No information side comprise 9% and 19% of the OFC population, respectively. There was little overlap between the cells comprising the CS versus US representations, for both information and water, in accord with observations that OFC encodes CSs and USs distinctly[11,41] (Extended Data Fig. 5f–k). Thus, significant numbers of OFC cells comprise each of the representations of the prediction and receipt of information and the prediction and receipt water reward.

https://doi.org/10.1038/s41593-026-02377-y

Distinct representations of intrinsic and extrinsic value

We have identified representations of each of the CS and US signals of information and water value in our task. We next determined whether these representations are distinct. We asked whether intrinsic and extrinsic value are represented differently in the recorded populations. This is of interest as these differences may result from the differential reinforcement of odor inputs predictive of information and water value. We first compared the information CS representation to the water CS representation (Extended Data Fig. 7a). We observed no correlation across cells between the information coding index at the center port odor and the water coding index at the side port odor (Pearson correlation $r = 0.04$, $P = 0.10$; Fig. 3a). In addition, there is only a small correlation between the information coding index at the side port odor that provides information (information US) and the water coding index at the receipt of water (water US) ($r = 0.08$, $P = 0.002$; Extended Data Fig. 7b). These data suggest that both the CS and US representations of information value and water value in our task are distinct.

The information and water value representations are evoked at different epochs within our task, and we considered that the distinct representations we observed might reflect this temporal separation[49]. We therefore designed a task in which representations of the predicted value of information and water could be analyzed at the same task epoch. We trained mice that had previously learned the information seeking task on a modified task in which four odors were presented at the center port. As in the original task, one odor directed the mouse to the Information side port and a second to the No information port. Two additional odors were presented, one signaling a large water amount (high value) at one side port and a second a small water amount (low value) at the other side port, each delivered with 100% probability (Fig. 3d). Mice displayed faster reaction times for information versus no information and high versus low value water reward trials, indicating they understood the meaning of the center port odors in this task ($P < 0.001$, Wilcoxon rank sum; Extended Data Fig. 7d).

We imaged OFC activity before and after concurrent reversal of the side locations for information and water value in this task and again pooled data for trial types balanced across sides. We then trained two different linear classifiers, one to decode information versus no information trials and one to decode high versus low water value trials at the center port, with trials for each classifier balanced across left and right side and pooled as pseudo-populations across animals (Fig. 3e,f). We were able to accurately decode information and water value prediction at the center port with these two separate classifiers (mean accuracy in 1 s post-odor 80% versus null 50%, $P < 0.001$, for information; 66% for water versus null 50%, $P < 0.001$; Fig. 3f). Thus, OFC represents both predicted information value and predicted water value in response to the different center port odors in this task.

In the original information seeking task, we observed highly correlated responses in OFC to the different center port odors on information forced and information choice trials ($r = 0.92$; Extended Data Fig. 6d). Similarly, in a previous study of associative learning[41], we demonstrated that responses in OFC to different odors predictive of water reward were highly correlated ($r = 0.80$). These observations imply that the responses to different odors predicting information or water represent predicted value rather than odor identity. We therefore compared responses to the odors predicting information and water reward value in the new information seeking task to understand whether information

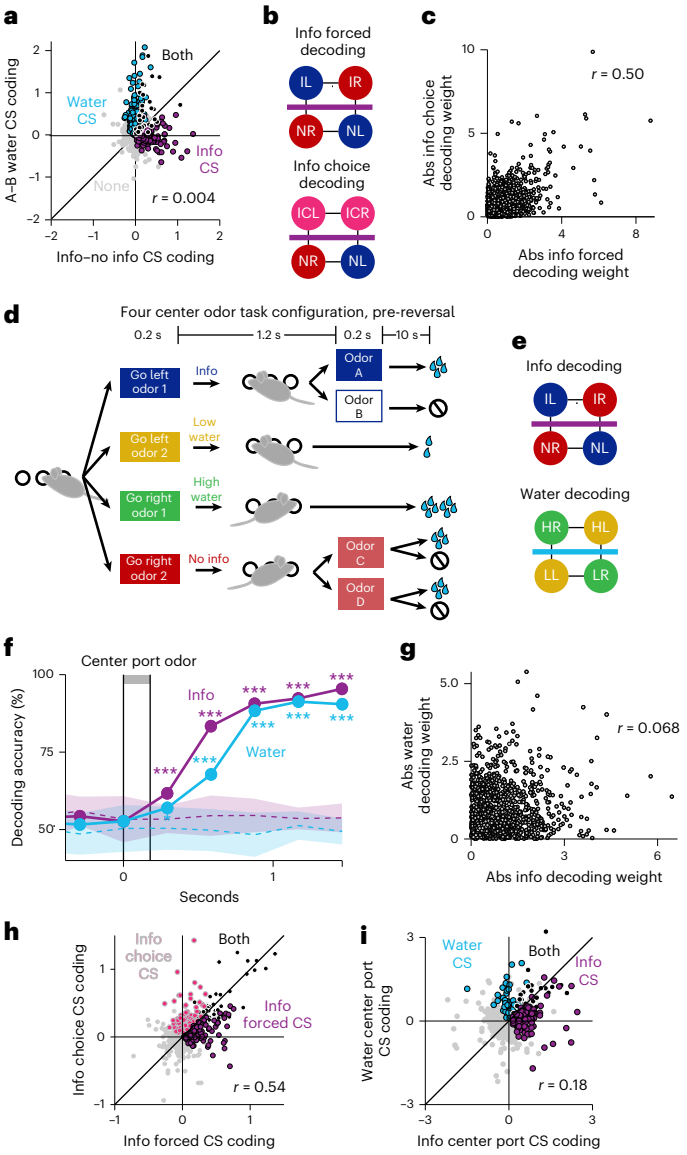

Fig. 3 | Representations of intrinsic and extrinsic value in OFC are distinct. **a**, The relationship between information CS coding (coding index 1 s after − 1 s before odor presentation at the center port) and water CS coding (coding index 1 s after − 1 s before odor presentation at the side port); two-sided Pearson correlation, $P = 0.87$, $N = 1138$ cells. **b**, Schematics for information forced and information choice decoding balanced across the left and right side. IL, info forced left; IR, info forced right; NR, no info forced right; NL, no info forced left; ICL, info choice left; ICR, info choice right; NR, no info forced right; NL, no info forced left. **c**, The relationship between information choice and information forced trial linear classifier decoding weights; two-sided Pearson correlation between mean absolute (abs) decoding weights across replicates, $P = 1.08 \times 10^{-72}$, $N = 1138$. **d**, Task-providing four center port odors that predict information, no information, large water reward (high value) and small water reward (low value). **e**, The decoding schematic for information versus no information and high versus low water value balanced across the left and right side. HR, high water value right; HL, high water value left; LL, low water value left; LR, low water value right. **f**, Information versus no information (purple) and high versus low water value (cyan) decoding accuracy. Lines show the pseudo-population with trials sampled across subjects and shading shows the shuffled null distributions. ***$P < 0.001$, one-tailed z score. Exact P values are listed in Supplementary Table 2. **g**, The relationship between information and water value decoding importance (absolute decoding weight); two-sided Pearson correlation between mean absolute (abs) decoding weights across replicates, $P = 0.036$, $N = 964$ cells. **h**, The relationship between information CS coding on forced information versus forced no information trials (coding index 1 s after − 1 s before odor presentation) and information CS coding on choice information versus forced no information trials (coding index 1 s after − 1 s before odor presentation); two-sided Pearson correlation, $P = 1.12 \times 10^{-87}$, $N = 1{,}138$ cells. **i**, The relationship in the four center odor task between information CS coding (coding index 1 s after − 1 s before odor presentation) and water CS coding (coding index 1 s after − 1 s before odor presentation) at the center port; two-sided Pearson correlation, $P = 2.73 \times 10^{-8}$, $N = 964$ cells.

and water value comprise distinct representations of value in OFC. We considered that if the encoding of information and water prediction reflects only a generalized signal shared across intrinsic and extrinsic value, representations of information and water value should be as similar to each other as representations of information value evoked by different odors. We therefore compared the information and water value classifiers we trained in the four center port odor task (Fig. 3d–f) to classifiers of information versus no information in forced and choice information trials, which are signaled by different odors in our original task (Fig. 2g and Extended Data Fig. 7c). We observed a correlation between each cell's weight in the classifier of information versus no information forced trials and the classifier of information choice versus no information forced trials ($r = 0.50$, $P < 0.0001$, Pearson correlation; Fig. 3c). By contrast, we observed a much smaller correlation between the decoding weights in the information and water value classifiers ($r = 0.068$, $P = 0.036$, Pearson correlation; Fig. 3g). Moreover, the angle of 49° between the axes of the information forced and information choice classifiers reflected similarity in neural state space, whereas the angle between the axes encoding information and water value, 99.9°, indicated near orthogonality of the axes in neural state space. The OFC representations of predicted information value in response to different odors are therefore more similar than representations of predicted information and water value. This implies that the representation of information value is distinct from the representation of water reward value in OFC.

In a separate analysis, we computed the information coding index and a water coding index for large versus small water reward trials in the new task (Extended Data Fig. 7e–g). We observed only a weak correlation between the CS predicting information and the CS predicting water value in the task with four center port odors ($r = 0.18$, $P < 0.0001$, Pearson correlation; Fig. 3i). By contrast, we observed a strong correlation in the coding indices for the information CS across forced and choice information trials in the original task ($r = 0.54$, $P < 0.0001$, Pearson correlation; Fig. 3h). The correlation between the information forced versus choice CS is 3.05 times larger than the correlation between the information and water CSs, providing further evidence for distinct information and water value representations. We performed a random shuffling of these data and observed that the probability of obtaining such a threefold difference in these correlations is 0.0054. Together, these data do not support a model of generalized value encoding that does not differentiate between intrinsic information and extrinsic water value, and instead provide evidence for distinct representations of predicted information and water in OFC.

OFC representation of predicted information scales with value

Our behavioral experiments show that as we diminish the delay between the side port odors and the receipt of water, mice diminish their preference for information. This suggests that the value of information is reduced with diminished delay[2,4,27,52]. We therefore examined the OFC responses to odors at the center port that predict information in sessions in our original task with either a 1 s or 10 s delay (Fig. 1k). Similar ensembles of cells exhibited information CS coding across both delays (45% overlap, $P < 0.001$, chi-square; Extended Data Fig. 8d). However, the magnitude of the information coding index for the center port odors was diminished in sessions with a 1-s delay (Fig. 4a–d). This reflected decreased responses to odors predictive of both information and no information (Extended Data Fig. 8a–c). The decrease in delay between information and reward outcome diminishes the duration of both knowledge and uncertainty, and this is reflected in the scaling of responses to both information and no information.

The decreased information coding index in sessions with a 1-s delay did not reflect a general decrease in value encoding in a shorter duration task, since no such difference was observed in the encoding of the water CS (Extended Data Fig. 8e) or US (Extended Data Fig. 8g) or the differential encoding of side odors C and D (Extended Data Fig. 8f). It also did not reflect instability in our tracking of cell identities across time or the addition of intervening training time, since it was not observed in matched sessions with a 10-s delay paired across an even longer intervening time period (Extended Data Fig. 8i). It was, however, replicated in a second set of 10-s versus 1-s sessions, in which the 1-s sessions occurred before the 10-s ones (Extended Data Fig. 8h). These data are in accord with our behavioral data and decision model that show a decreased preference for information with shorter delay and suggest that the information CS representation reflects the intrinsic value of information as scaled by delay.

The emergence of representations of information value with learning

We recorded the emergence of representations of the value of information as mice learned that information was available at one of the two side ports. During early training, before exposure to informative odor, the two different center port odors directed movement to the left or right port, where mice received equal water reward on every trial (Extended Data Fig. 8j). Information-providing odors were then introduced and water was delivered with 25% probability at both ports (Extended Data Fig. 8j). Thus, mice learned that one port provided information as to whether they would receive water reward.

We observed increased differential activity in response to odors at the center port upon learning. We computed the coding index from differential activity at the center port between left and right side trials before learning. After learning, the odor that previously directed the mouse to the left port, for example, now also predicted information at the left port, whereas the odor directing the mouse to the right port now predicted no information. We computed the information coding index from the differential activity at the center port after learning. We observed that the information coding index after learning is greater than the coding index between left and right before learning (Fig. 4e–h). This increase is due to an enhanced response to odors predictive of information in cells that overlap with those that previously responded to those odors before learning (increased response to information $P < 0.001$, sign-rank test, 55% overlap, $P < 0.001$, chi-square; Fig. 4e and Extended Data Fig. 8k–m). Thus, a representation predictive of information emerges from the ensemble of cells that previously represented odor directing the mouse to a particular side to receive water reward.

We also observed the emergence of the US representation of information at the side port with learning. The coding index reflecting differential activity at the side port increased upon the introduction of the side port odors and information (Extended Data Fig. 8n). This provides further evidence that the difference in response to the information side port odors A and B compared to the no information side port odors C and D reflects the receipt of information, an information US, and not a continuation of the center port odor CS response or entry into the side port.

Representations of intrinsic and extrinsic value in low-dimensional population dynamics

We identified representations of intrinsic information and extrinsic water value at particular epochs in the information seeking task. We also asked whether we could identify these value representations as latent variables in the dynamic unfolding of activity in OFC throughout the task. We fit a latent variable model called consistent embeddings of high-dimensional recordings using auxiliary variables (CEBRA)[53] to derive task-relevant low-dimensional embedding spaces by jointly fitting neural data and behavioral labels across animals in our original task (Fig. 5a–i and Extended Data Fig. 9). We observed that the differences between information and no information and reward and no reward trials could be decoded from low-dimensional CEBRA manifold embeddings (Fig. 5j–l and Extended Data Fig. 9). We also modeled OFC activity across sessions with 1-s versus 10-s delays between information

https://doi.org/10.1038/s41593-026-02377-y

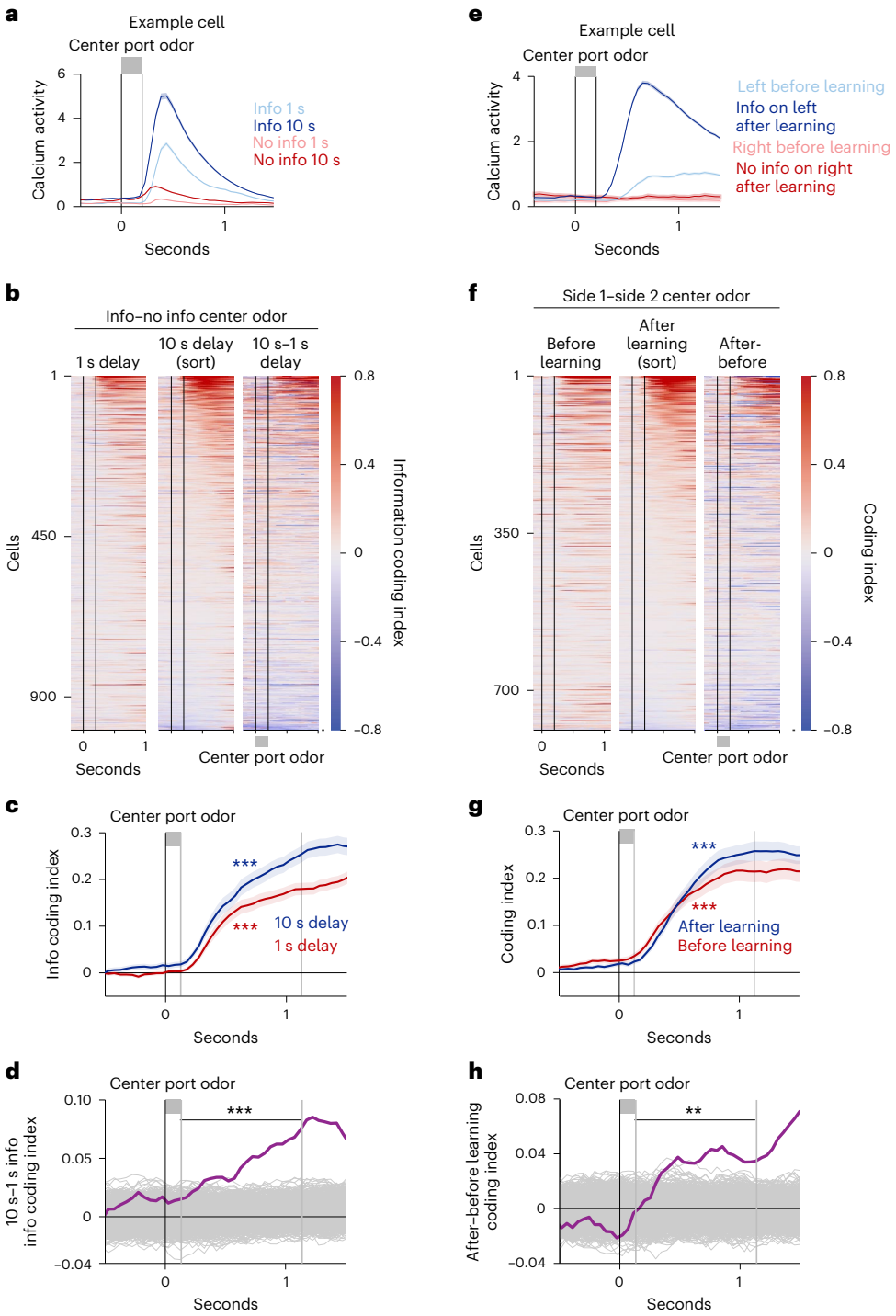

Fig. 4 | OFC representations of predicted information reflect the intrinsic value of information and emerge with learning. a, The activity of an example cell at center port odor in sessions with a 1-s versus a 10-s delay. The line shows the mean and shading shows s.e.m. **b**, The information coding index across the population in sessions with a 1-s delay, 10-s delay and their difference. Cells across all columns are sorted by values in 10-s delay. **c**, The population mean information coding index at the center port in sessions with a 1-s versus a 10-s delay. Mean and s.e.m. shown. ***$P < 0.001$, permutation test on coding index 1 s after −1 s before odor presentation, trial sample sizes in Supplementary Table 5. **d**, The difference between information coding index at the center port in 10-s − 1-s delay sessions (purple). Gray shows shuffled data, ***$P < 0.001$, permutation test, trial sample sizes in Supplementary Table 5. **e**, The activity of an example cell at center port odor in sessions before and after the introduction of information and probabilistic reward, plot as in **a**. **f**, The population mean coding index at center port odor on forced left − forced right trials before learning, forced information − forced no information trials after learning and their difference. Cells across all columns are sorted by values after learning. **g**, The population mean coding index at the center port for the left − right side in sessions before learning and information − no information in sessions after learning. Mean and s.e.m. shown. ***$P < 0.001$, permutation test on coding index 1 s after −1 s before odor presentation, trial sample sizes in Supplementary Table 4. **h**, The difference between coding index at the center port before and after learning (purple). Gray shows shuffled data, **$P = 0.024$, permutation test, trial sample sizes in Supplementary Table 4.

https://doi.org/10.1038/s41593-026-02377-y

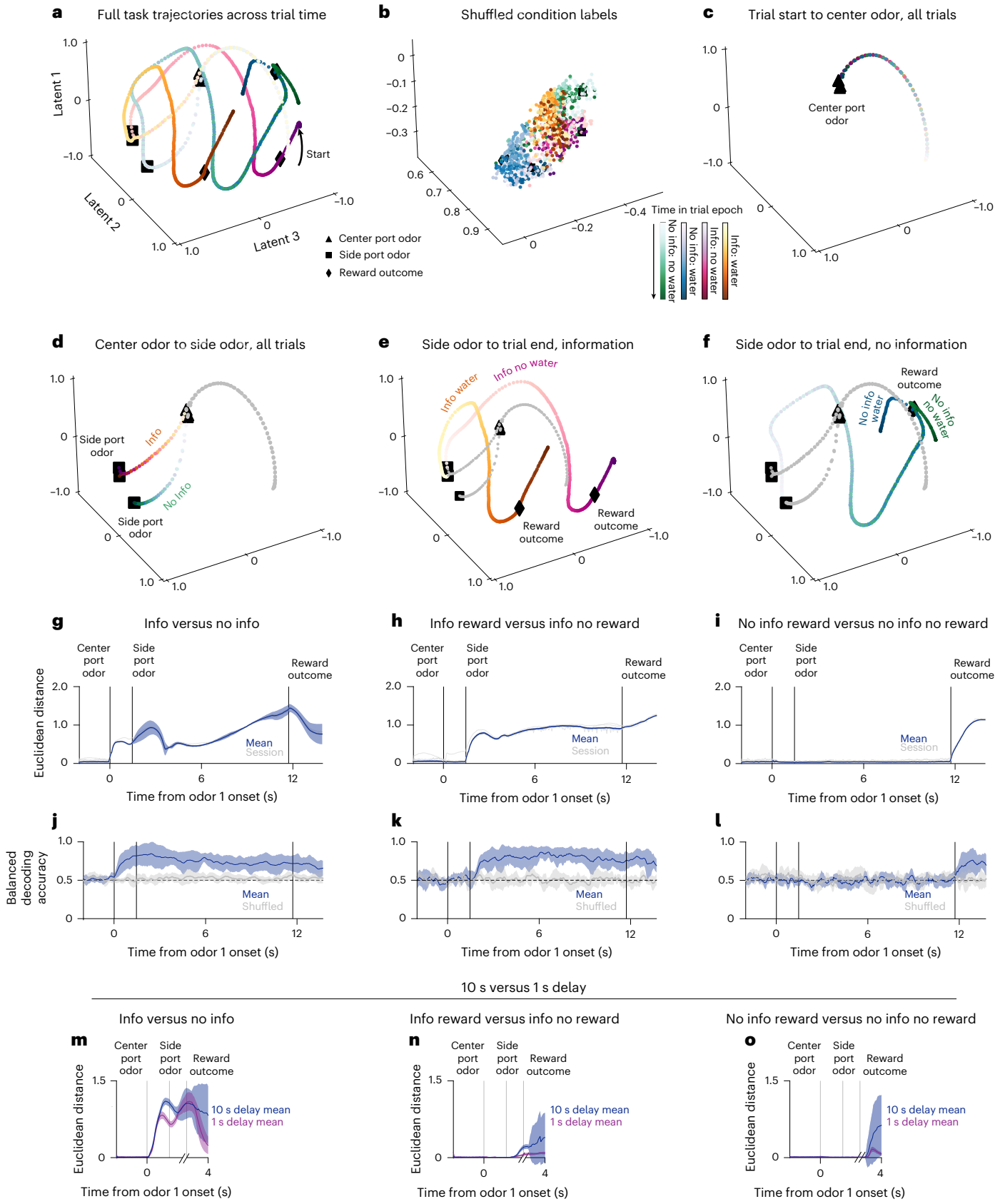

and water reward and observed decreased distance between the CEBRA embeddings of information and no information trials in sessions with 1-s delay (Fig. 5m–o). The ability to decode information versus no information and reward versus no reward trials from the CEBRA model fit concurrently across all animals suggests that these two kinds of value are represented in OFC neural dynamics on a low-dimensional manifold during performance of the information seeking task. These analyses further support the idea that mice compute and maintain

Fig. 5 | CEBRA model reveals dynamic manifold encoding of information and water value. a, The first three latents of CEBRA embedding across trial time (from light to dark) for interacting labels of information and reward in a single session for a single animal. **b**, Plot as in **a** for data with maximally shuffled labels. **c**–**f**, CEBRA embeddings by trial epochs (points shaded from light to dark to indicate time) for trial start to center odor (all trials) (**c**), center odor to side odor (all trials) (**d**), side odor to trial end (information) (**e**) and side odor to trial end (no information (**f**). **g**–**i**, Euclidean distance between trial type trajectories in CEBRA embeddings for information versus no information (**g**), information reward versus information no reward (**h**) and no information reward versus no information no reward (**i**). The line shows the mean and shading shows 95% CI across cross-validation folds. **j**–**l**, Decoding of trial types from CEBRA embeddings for information versus no information (**j**), information reward versus information no reward (**k**) and no information reward versus no information no reward (**l**). The line shows mean and shading shows 95% CI across cross-validation folds. **m**–**o**, The Euclidean distance in model jointly fitting sessions with a 1-s and 10-s delay between information and water reward outcome for information versus no information (**m**), information reward versus information no reward (**n**) and no information reward versus no information no reward (**o**).

separate representations of information and water value when seeking information about water reward.

Discussion

We have developed a behavioral paradigm that demonstrates that mice choose to acquire information even though this information does not alter the reward outcome of the task. Moreover, mice are willing to sacrifice water reward for information, suggesting that in mice, as in several other species, information is of intrinsic value[2–6,9,10,15,21,22,54]. Our paradigm has enabled the study of information seeking behavior in mice, allowing the use of methods that are not available in other information seeking species such as monkeys or humans.

Longitudinal calcium imaging during the information seeking task allowed us to follow the emergence of a representation of predicted information value during learning at the level of population structure. We observed that the representation of predicted information elicited by odor reflects information value scaled by delay, which our decision model suggests mice calculate separately from water reward. Moreover, we observed distinct representations of odors predicting information value and odors predicting water value along separate decoding dimensions in both linear classifiers at specific task epochs and on a manifold within OFC dynamics. These data suggest that mice have evolved dedicated pathways in OFC that represent the intrinsic value of information and the extrinsic value of water reward. Electrophysiological recordings in monkeys during an information seeking task conceptually analogous to our paradigm similarly reveal orthogonal coding of information and water reward in single neurons in OFC[11]. The presence of distinct representations within OFC may allow the organism to separately learn and update different elements of a rewarding stimulus and execute different behaviors in response to distinct value representations.

Representations of the value of information must involve a complex process of cognitive abstraction because recognition that an odor provides information requires knowledge of its predictive nature despite the lack of its association with an external reward. Indeed, we observed a representation of odors that provide information irrespective of the water value associated with this information. This poses the question as to how the brain initially recognizes that an odor cue provides information of intrinsic value. Models of classical conditioning involving rewards of extrinsic value, such as food or water, invoke known physiologic responses that activate subcortical brain structures that lead to the release of dopamine and downstream reinforcement[17–19]. Analogous models for rewards of intrinsic value suggest that in our information seeking task, there must be an odor-responsive neural ensemble that encodes the value of information and is capable of reinforcing information-predictive odor cues in OFC. However, the nature of the brain structures capable of recognizing the innate value of information and reinforcing a distinct OFC population remains elusive[11,26].

Why does an organism value information of no apparent extrinsic value? One class of models argues that information seeking is a consequence of secondary reinforcement[5,55–61]. The receipt of odor A (the odor predictive of water reward) at the information side port may be overvalued and secondarily reinforce the choice of information at the center port. A second model posits that odor A at the side port boosts 'anticipatory delight' enhancing the value of the information port[2]. These models may not easily account for observations that humans and other animals exhibit a desire for information about upcoming aversive events and events that have already occurred[10,22,62–64]. Others have argued that the resolution of the aversion of uncertainty provides a basis for the value of information[27,61,62,65–69]. Perhaps the simplest explanation argues that information led, at some time during the evolution of a species, to extrinsic value. Indeed, in natural environments, knowledge improves an organism's model of the world, and its acquisition improves decision making and augments survival[38,70]. This quest for information may therefore have been fixed by selection and now generalizes to circumstances in which the acquisition of knowledge may be of no extrinsic value. This model suggests that the desire for knowledge evolved by assigning innate pleasure to the acquisition of information. Thus, the value of information may ultimately reflect the pleasure it provides.

Online content

Any methods, additional references, Nature Portfolio reporting summaries, source data, extended data, supplementary information, acknowledgements, peer review information; details of author contributions and competing interests; and statements of data and code availability are available at https://doi.org/10.1038/s41593-026-02377-y.

References

1. Jezzini, A., Bromberg-Martin, E. S., Trambaiolli, L. R., Haber, S. N. & Monosov, I. E. A prefrontal network integrates preferences for advance information about uncertain rewards and punishments. *Neuron* **109**, 2339–2352.e5 (2021).
2. Iigaya, K., Story, G. W., Kurth-Nelson, Z., Dolan, R. J. & Dayan, P. The modulation of savouring by prediction error and its effects on choice. *eLife* **5**, e13747 (2016).
3. Roper, K. L. & Zentall, T. R. Observing behavior in pigeons: the effect of reinforcement probability and response cost using a symmetrical choice procedure. *Learn. Motiv.* **30**, 201–220 (1999).
4. McDevitt, M. A., Pisklak, J. M., Spetch, M. & Dunn, R. The influence of outcome delay on suboptimal choice. *Behav. Process.* **157**, 279–285 (2018).
5. Ajuwon, V., Ojeda, A., Murphy, R. A., Monteiro, T. & Kacelnik, A. Paradoxical choice and the reinforcing value of information. *Anim. Cogn.* **26**, 623–637 (2023).
6. Ojeda, A., Murphy, R. A. & Kacelnik, A. Paradoxical choice in rats: subjective valuation and mechanism of choice. *Behav. Process.* **152**, 73–80 (2018).
7. Zhu, J.-Q., Xiang, W. & Ludvig, E. A. Information seeking as chasing anticipated prediction errors. In *Proc. 39th Annual Meeting of the Cognitive Science Society* **39**, 3658–663 (2017).
8. Roper, K. L. & Baldwin, E. R. The two-alternative observing response procedure in rats: preference for nondiscriminative stimuli and the effect of delay. *Learn. Motiv.* **35**, 275–302 (2004).
9. González, V. V. et al. A special role for anterior cingulate cortex, but not orbitofrontal cortex or basolateral amygdala, in choices involving information. *Cereb. Cortex* **34**, bhae135 (2024).

10. Kobayashi, K. & Hsu, M. Common neural code for reward and information value. *Proc. Natl Acad. Sci. USA* **116**, 13061–13066 (2019).
11. Blanchard, T. C., Hayden, B. Y. & Bromberg-Martin, E. S. Orbitofrontal cortex uses distinct codes for different choice attributes in decisions motivated by curiosity. *Neuron* **85**, 602–614 (2015).
12. Bennett, D., Bode, S., Brydevall, M., Warren, H. & Murawski, C. Intrinsic valuation of information in decision making under uncertainty. *PLoS Comput. Biol.* **12**, e1005020 (2016).
13. Rodriguez Cabrero, J. A. M., Zhu, J.-Q. & Ludvig, E. A. Costly curiosity: people pay a price to resolve an uncertain gamble early. *Behav. Process.* **160**, 20–25 (2019).
14. Cunningham, P. J. & Shahan, T. A. Rats engage in suboptimal choice when the delay to food is sufficiently long. *J. Exp. Psychol. Anim. Learn. Cogn.* **45**, 301–310 (2019).
15. Bromberg-Martin, E. S. & Hikosaka, O. Midbrain dopamine neurons signal preference for advance information about upcoming rewards. *Neuron* **63**, 119–126 (2009).
16. Murayama, K. A reward-learning framework of knowledge acquisition: an integrated account of curiosity, interest, and intrinsic–extrinsic rewards. *Psychol. Rev.* **129**, 175–198 (2022).
17. Grove, J. C. R. et al. Dopamine subsystems that track internal states. *Nature* **608**, 374–380 (2022).
18. Araujo, I. E. de, Schatzker, M. & Small, D. M. Rethinking food reward. *Annu. Rev. Psychol.* **71**, 139–164 (2020).
19. Alcantara, I. C., Tapia, A. P. M., Aponte, Y. & Krashes, M. J. Acts of appetite: neural circuits governing the appetitive, consummatory, and terminating phases of feeding. *Nat. Metab.* **4**, 836–847 (2022).
20. Iigaya, K. et al. The value of what's to come: neural mechanisms coupling prediction error and the utility of anticipation. *Sci. Adv.* **6**, eaba3828 (2020).
21. Cogliati Dezza, I., Cleeremans, A. & Alexander, W. H. Independent and interacting value systems for reward and information in the human brain. *eLife* **11**, e66358 (2022).
22. Charpentier, C. J., Bromberg-Martin, E. S. & Sharot, T. Valuation of knowledge and ignorance in mesolimbic reward circuitry. *Proc. Natl Acad. Sci. USA* **115**, E7255–E7264 (2018).
23. van Lieshout, L. L. F., Vandenbroucke, A. R. E., Müller, N. C. J., Cools, R. & de Lange, F. P. Induction and relief of curiosity elicit parietal and frontal activity. *J. Neurosci.* **38**, 2579–2588 (2018).
24. Kaanders, P., Nili, H., O'Reilly, J. X. & Hunt, L. Medial frontal cortex activity predicts information sampling in economic choice. *J. Neurosci.* **41**, 8403–8413 (2021).
25. Jessup, R. K. & O'Doherty, J. P. Distinguishing informational from value-related encoding of rewarding and punishing outcomes in the human brain. *Eur. J. Neurosci.* **39**, 2014–2026 (2014).
26. White, J. K. et al. A neural network for information seeking. *Nat. Commun.* **10**, 1–19 (2019).
27. Bromberg-Martin, E. S. et al. A neural mechanism for conserved value computations integrating information and rewards. *Nat. Neurosci.* **27**, 159–175 (2024).
28. Hayden, B. Y. & Niv, Y. The case against economic values in the orbitofrontal cortex (or anywhere else in the brain). *Behav. Neurosci.* **135**, 192–201 (2021).
29. Padoa-Schioppa, C. & Assad, J. A. Neurons in the orbitofrontal cortex encode economic value. *Nature* **441**, 223–226 (2006).
30. Ballesta, S., Shi, W., Conen, K. E. & Padoa-Schioppa, C. Values encoded in orbitofrontal cortex are causally related to economic choices. *Nature* **588**, 450–453 (2020).
31. Kuwabara, M., Kang, N., Holy, T. E. & Padoa-Schioppa, C. Neural mechanisms of economic choices in mice. *eLife* **9**, e49669 (2020).
32. Wilson, R. C., Takahashi, Y. K., Schoenbaum, G. & Niv, Y. Orbitofrontal cortex as a cognitive map of task space. *Neuron* **81**, 267–279 (2014).
33. Stalnaker, T. A., Cooch, N. K. & Schoenbaum, G. What the orbitofrontal cortex does not do. *Nat. Neurosci.* **18**, 620–627 (2015).
34. Kable, J. W. & Glimcher, P. W. The neural correlates of subjective value during intertemporal choice. *Nat. Neurosci.* **10**, 1625–1633 (2007).
35. Ottenheimer, D. J., Hjort, M. M., Bowen, A. J., Steinmetz, N. A. & Stuber, G. D. A stable, distributed code for cue value in mouse cortex during reward learning. *eLife* **12**, RP84604 (2023).
36. Cai, X., Kim, S. & Lee, D. Heterogeneous coding of temporally discounted values in the dorsal and ventral striatum during intertemporal choice. *Neuron* **69**, 170–182 (2011).
37. Eliaz, K. & Schotter, A. Paying for confidence: an experimental study of the demand for non-instrumental information. *Games Econ. Behav.* **70**, 304–324 (2010).
38. Bromberg-Martin, E. S. & Monosov, I. E. Neural circuitry of information seeking. *Curr. Opin. Behav. Sci.* **35**, 62–70 (2020).
39. Rescorla, R. A. & Wagner, A. R. A theory of Pavlovian conditioning: Variations in the effectiveness of reinforcement and nonreinforcement. In *Classical Conditioning II: Current Research and Theory* (eds Black, A. H. & Prokasy, W. F.) 64–99 (Appleton-Century-Crofts, 1972).
40. Dezza, I. C., Yu, A. J., Cleeremans, A. & Alexander, W. Learning the value of information and reward over time when solving exploration-exploitation problems. *Sci. Rep.* **7**, 16919 (2017).
41. Wang, P. Y. et al. Transient and persistent representations of odor value in prefrontal cortex. *Neuron* **108**, 209–224.e6 (2020).
42. Padoa-Schioppa, C. Orbitofrontal cortex and the computation of economic value. *Ann. N. Y. Acad. Sci.* **1121**, 232–253 (2007).
43. Gore, F. et al. Orbitofrontal cortex control of striatum leads economic decision-making. *Nat. Neurosci.* **26**, 1566–1574 (2023).
44. Schoenbaum, G., Takahashi, Y., Liu, T.-L. & McDannald, M. A. Does the orbitofrontal cortex signal value?. *Ann. N. Y. Acad. Sci.* **1239**, 87–99 (2011).
45. Ramus, S. J. & Eichenbaum, H. Neural correlates of olfactory recognition memory in the rat orbitofrontal cortex. *J. Neurosci.* **20**, 8199–8208 (2000).
46. Feierstein, C. E., Quirk, M. C., Uchida, N., Sosulski, D. L. & Mainen, Z. F. Representation of spatial goals in rat orbitofrontal cortex. *Neuron* **51**, 495–507 (2006).
47. Basu, R. et al. The orbitofrontal cortex maps future navigational goals. *Nature* **599**, 449–452 (2021).
48. Wikenheiser, A. M., Gardner, M. P. H., Mueller, L. E. & Schoenbaum, G. Spatial representations in rat orbitofrontal cortex. *J. Neurosci.* **41**, 6933–6945 (2021).
49. Zhou, J. et al. Rat orbitofrontal ensemble activity contains multiplexed but dissociable representations of value and task structure in an odor sequence task. *Curr. Biol.* **29**, 897–907.e3 (2019).
50. Fusi, S., Miller, E. K. & Rigotti, M. Why neurons mix: high dimensionality for higher cognition. *Curr. Opin. Neurobiol.* **37**, 66–74 (2016).
51. Zhang, M. et al. The representation of decision variables in orbitofrontal cortex is longitudinally stable. *Cell Reports* **43**, 114772 (2024).
52. Vasconcelos, M., Monteiro, T. & Kacelnik, A. Irrational choice and the value of information. *Sci. Rep.* **5**, 13874 (2015).
53. Schneider, S., Lee, J. H. & Mathis, M. W. Learnable latent embeddings for joint behavioural and neural analysis. *Nature* **617**, 360–368 (2023).
54. Li, Y., Daddaoua, N., Horan, M., Foley, N. C. & Gottlieb, J. Uncertainty modulates visual maps during noninstrumental information demand. *Nat. Commun.* **13**, 5911 (2022).
55. Lieberman, D. A. Secondary reinforcement and information as determinants of observing behavior in monkeys (*Macaca mulatta*). *Learn. Motiv.* **3**, 341–358 (1972).
56. Beierholm, U. R. & Dayan, P. Pavlovian-instrumental interaction in 'observing behavior'. *PLoS Comput. Biol.* **6**, e1000903 (2010).

57. Dunn, R. M., Pisklak, J. M., McDevitt, M. A. & Spetch, M. L. Suboptimal choice: a review and quantification of the signal for good news (SiGN) model. *Psychol. Rev.* **131**, 58–78 (2024).
58. Chow, J. J., Smith, A. P., Wilson, A. G., Zentall, T. R. & Beckmann, J. S. Suboptimal choice in rats: incentive salience attribution promotes maladaptive decision-making. *Behav. Brain Res.* **320**, 244–254 (2017).
59. Fantino, E. & Moore, J. Uncertainty reduction, conditioned reinforcement, and observing. *J. Exp. Anal. Behav.* **33**, 3–13 (1980).
60. González, V. V. & Blaisdell, A. P. Inhibition and paradoxical choice. *Learn. Behav.* **51**, 458–467 (2023).
61. Daddaoua, N., Lopes, M. & Gottlieb, J. Intrinsically motivated oculomotor exploration guided by uncertainty reduction and conditioned reinforcement in non-human primates. *Sci. Rep.* **6**, 20202 (2016).
62. Wang, M. Z. & Hayden, B. Y. Monkeys are curious about counterfactual outcomes. *Cognition* **189**, 1–10 (2019).
63. Marvin, C. B. & Shohamy, D. Curiosity and reward: valence predicts choice and information prediction errors enhance learning. *J. Exp. Psychol. Gen.* **145**, 266–272 (2016).
64. FitzGibbon, L., Komiya, A. & Murayama, K. The lure of counterfactual curiosity: people incur a cost to experience regret. *Psychol. Sci.* **32**, 241–255 (2021).
65. Friston, K. et al. Active inference and epistemic value. *Cogn. Neurosci.* **6**, 187–214 (2015).
66. Berlyne, D. E. Uncertainty and epistemic curiosity. *Br. J. Psychol.* **53**, 27–34 (1962).
67. Berlyne, D. E. Novelty and curiosity as determinants of exploratory behaviour. *Br. J. Psychol. Gen. Sect.* **41**, 68–80 (1950).
68. Loewenstein, G. The psychology of curiosity: a review and reinterpretation. *Psychol. Bull.* **116**, 75–98 (1994).
69. Golman, R. & Loewenstein, G. *Curiosity, Information Gaps, and the Utility of Knowledge* (SSRN, 2015); https://papers.ssrn.com/abstract=2149362
70. Behrens, T. E. J., Woolrich, M. W., Walton, M. E. & Rushworth, M. F. S. Learning the value of information in an uncertain world. *Nat. Neurosci.* **10**, 1214–1221 (2007).

Methods

Subjects

All experimental and surgical protocols were performed in accordance with the guide of Care and Use of Laboratory Animals (NIH) and were approved by the Institutional Animal Care and Use Committee at Columbia University. Mice were wild-type C57/BL6 (Jackson Laboratories strain 000664), aged 8–45 weeks, of both male and female sex. Mice were water restricted at least 2 days before the initiation of training and maintained at >80% of their initial body weight throughout experiments. Mice were handled by experimenters for approximately 5–15 min for at least 2 days before beginning behavioral training. All animals were maintained under reverse cycled 12 h light/12 h dark conditions and single housed after beginning water restriction. Experiments were performed during the dark period of the circadian cycle.

Behavior training and testing

In general, mice were trained on the information seeking task in one session for 45–100 min each weekday. Training sessions lasted until mice received at least 700 µl of water or stopped engaging in trials. On average, mice received 800–1400 µl of water per session and received water later that day in their home cage if daily requirements were not met during training.

Main task. Mice were trained to perform a two-alternative forced-choice task in which they chose whether to receive information revealing the trial's reward outcome (water or no water). Behavioral training and testing were performed in custom-made acrylic boxes outfitted with three nosepoke ports (Sanworks) with odor and water delivery spouts and a solenoid valve (The Lee Company, LHDB1233418H) to deliver the water reward along one wall in custom sound- and light-attenuating enclosures (MBkit). The boxes also contained a speaker to deliver audio cues (tones). Tones were controlled by a Bpod HiFi module and played through a speaker (Peerless, Tymphany XT25SC90-04) and an amplifier board (AMP2X15, PUI Audio). Behavioral hardware was controlled using Bpod microcontrollers.

In the information seeking task, mice initiated trials by poking an illuminated center nosepoke port where one of three trial type odor cues was provided for 200 ms. Following a 50-ms 4,500-Hz go cue tone, the center port light went out and mice then chose either information or no information by poking into either the left or right reward port to trigger its infrared sensor. Each animal was initially assigned either left or right as the information port, pseudo-randomized across animals. Mice had to indicate their choice before the delivery of a 200-ms odor cue in the chosen side port 1.2 s after the completion of the go cue or the trial had to be repeated after allowing the remainder of its duration to elapse. On some training sessions, a grace period of up to 10 s was provided to extend the time available for the mouse to indicate its choice. In this case, the side odor was presented as soon as the mouse entered the correct side port. If mice did not stay in the center nosepoke for the duration of the center odor delivery and go cue, they were unable to proceed with the trial and had to repoke the center port for the full odor duration to proceed. After initial training (see details below), trials were of three types presented in pseudo-random order in blocks of 12: forced information, forced no information and choice. If mice chose the incorrect port on forced trials, they did not receive side port odor or reward and experienced an uncued timeout for the remainder of the full trial time and had to repeat the trial. These procedures ensured mice were unable to avoid nonpreferred trial types and equalized reward rates across trial types during training.

At the side ports, on each trial mice received one of four odors for 200 ms: the information port provided odor A on 25% of trials, which was always followed by water reward, or odor B on 75% of trials, which was never followed by a water reward. The no information port provided odor C on 75% of trials and odor D on 25% of trials, but the water reward was determined independently and provided on 25% of no information trials. The unequal frequency of odors C and D was designed to control for possible frequency effects on the neural representations of the side port odors A and B unassociated with their prediction of water value. The delivery of the side odor was followed by a delay period of 10 s in the main task. A 4,000-Hz 200-ms tone then indicated the outcome time on all trials, although water was only provided at that time on rewarded trials. Water rewards in the main task were 16 µl provided as 4 × 4 µl drops 50 ms apart. Unrewarded trials provided a time delay to match the duration of water delivery. The reward outcome period was followed by a 3-s intertrial interval. Mice were required to be present in the chosen port for water to be delivered, but they were not otherwise required to be in the port after indicating their choice.

All odors used in the task were monomolecular neutral odorants diluted in mineral oil, through which compressed medical-grade air was bubbled in custom-built olfactometers using mass flow controllers (Aalborg, GFCS-010201) and solenoid valves (The Lee Company, LHQA1221220H), whose opening was controlled by the Bpod system valve modules. Each odor bottle had a valve located before and after it to ensure accurate odor delivery timing. An odor line of 333 ml min^{-1} was combined with a carrier line of 333 ml min^{-1} to deliver a total air flow rate of approximately 667 ml min^{-1} into each of the three nosepoke ports. Air flow was maintained at the same rate but passed through a mineral oil control when odor stimuli were not being delivered. Odor identities were randomized across animals among four odors able to be delivered to the center port and four odors able to be delivered to either side port. Latch valves (The Lee Company, LHLA1221211H) switched odor delivery across the left and right sides. Odors were obtained at >98% purity from Sigma-Aldrich. Odors and concentrations used were as follows, at the center port: isoamyl acetate (1:10), pinene (1:5), benzaldehyde (1:10), limonene (1:5); at the side port: ethyl butyrate (1:20), acetophenone (1:5), octanal (1:5), *cis*-3-hexen-1-ol (1:10).

Behavior and olfactometer hardware were controlled by Bpod microcontroller systems (Sanworks, Finite State Machine r2.5) and their MATLAB interface as well as custom MATLAB code (Mathworks). Behavioral timestamps, video recording and imaging frame acquisition were synchronized using external data acquisition systems (National Instruments, USB-6002).

Behavioral training. Mice were trained to perform the information seeking task over several weeks of behavioral shaping progressing through the following stages.

1. Covered side training (Extended Data Fig. 1a). Mice performed alternating blocks of trials where they had to trigger the center port and then enter the left or right port where they received water reward. The incorrect port was covered to prevent entry for the duration of each block of ~50 trials (200 µl total reward) each. Trials provided one to two drops of 4 µl of water, with the reward on the two sides being equal. The center port odors that would direct mice to each side on later forced trials were presented for the duration of the mouse's triggering of the center port, and the duration of the center poke required to trigger the start of the trial was gradually increased to 200 ms. Delivery of water at the side port was delayed up to 1 s with gradual increases as mice became proficient at this training stage. The 3-s intertrial interval was also introduced to decrease repetitive behavior. Mice progressed to the next training stage when they achieved >50% complete trial initiations (remaining for the full 200 ms of center port odor presentation) and had rapid reaction times (<2 s).
2. Uncovered side training (Extended Data Fig. 1b). This stage was not always included but was implemented for animals that had not fully learned the association between center port odors and the required forced side location. Mice completed blocks of

~20–50 trials directed to the left or right side by the odor provided in the center port with the incorrect side uncovered and accessible. They only received water if they chose the correct side port.

3. Delay training (Extended Data Fig. 1b). Mice next performed trials with all ports uncovered and pseudo-randomly alternating forced left and right trials with the center port odor directing them to the left or the right. All correctly chosen trials were rewarded (one to two 4 µl drops) equally on the two sides. The delay between the completion of trial initiation at the center port and water reward delivery following correct choice of the side port was gradually increased by 200–1,000 ms approximately every 50 trials until the full delay value of 10 s was reached. Delays were increased manually while observing mouse behavior to moderate task difficulty and ensure animals maintained adequate motivation. During this stage, a reaction time requirement was instituted such that mice must choose the correct port within a certain amount of time to receive reward. This time was gradually decreased to the final value of 1.2 s. Mice moved on to the next training stage when they achieved >70% correct performance at the full delay value.
4. Introduction of information (Extended Data Fig. 1c). In the next stage, trial rewards became probabilistic, and side port odors were introduced. Reward probability was decreased to 50% on all trials. Two hundred milisecond presentations of the side port odors (A, B, C and D) occurred 1.2 s after the go cue in the correctly chosen side port with the appropriate contingencies, such that odor A was always followed by water reward, odor B was never rewarded and odors C and D were each followed by water reward on 50% of trials. This allowed mice to begin learning that A and B resolved the trial's outcome and provided information, while C and D did not provide information. Two to three sessions were performed at 50% reward and then the reward probability was dropped to 25%. Licking responses and the mouse's presence in the reward port were monitored to ensure they were learning the meanings of the side port odors (mice tended to leave the side port following receipt of odor B). This training stage lasted five to seven sessions to ensure all mice learned that information was provided.
5. Choice training (Extended Data Fig. 1d). Mice were explicitly taught that the choice center port odor allowed them to receive equal probability water reward at either side port in this stage of training. Task event times, side port odors and reward probabilities were the same as in the previous stage. Mice performed blocks of 10–50 trials with one side port covered to prevent accessing it. Trials with the appropriate forced odor (Information or No Information) for the uncovered side were alternated pseudo-randomly with trials in which the new choice odor was presented at the center port. Blocks were alternated to ensure mice experienced equal reward rates and total reward amounts following the choice odor on the left and right side to minimize side bias. This stage lasted for five to seven sessions, or ~250–300 choice trials on each side.
6. Full task/preference measurement (Fig. 1a). Following choice training, mice were tested for preference for information on the full version of the task. Both side ports were uncovered and mice performed all three trial types: forced information, forced no information and choice, pseudo-randomly interleaved throughout each session. Trial types were set in blocks of 12 to ensure mice performed roughly equal numbers of trials of each type within a session, and rewards were assigned in blocks of 8 since trials were rewarded with 25% probability to ensure mice were rewarded frequently enough to maintain their motivation to engage in the task. In initial behavioral tests ($n = 14$), preference was tested for three sessions, then the side identities were reversed. Some mice ($n = 7$) performed two additional side reversals such that their preference was tested with information twice on each side for three sessions. In mice that were imaged and subsequent mice ($n = 15$), preference was tested for 6 days on each side to ensure stabilized learning of the relevant neural representations. On side reversals, the side locations of the information and no information side port odors were switched while center port odors still indicated movement to the same side. This meant that the center port odor that had previously signaled Information on the left side and was followed by odor A or odor B now signaled No information on the left side and was followed by odor C or odor D. Similarly, mice had to learn that Information had moved from the right to the left side or vice versa.

Water and delay titration experiments. Following side reversals, information was returned to the initial side port and mice were trained for several more sessions (~3) until their preference restabilized. Mice that had displayed information preference on both sides were then tested as follows in water ($N = 4$) and/or delay titration ($N = 6$) experiments (Fig. 1i–l). A stairstep procedure was used to determine the willingness of mice to sacrifice water reward for information. The reward probability on both sides was raised to 50%, but the reward amount on the information side was changed for 3 sessions at a time. Reward values of 4-µl drops were one drop, six drops, two drops, five drops, three drops and four drops, and then these amounts were retested in reverse order. Preference was calculated as the mean across the final session in each block at a given reward amount, such that two sessions were used to calculate the preference at each reward amount. Sessions with six drops were omitted from plotting and modeling due to ceiling effects. A similar procedure, but for single blocks of 6 days at each value, was used for imaged mice.

Information preference was measured across different durations of the delay between side odor presentation and water reward using a similar procedure in which preference was tested for 6 days at each delay value: 1 s, 10 s, 4 s, 10 s and 6 s. Preference was determined as the mean preference for information in the last two sessions at each delay value.

Task with reward cues on all trials. The task was modified to explicitly cue mice when reward would be revealed so that they learned they could leave the side port on all trials (Extended Data Fig. 2). In all stages of this training, after mice experienced 80% of the delay length between the side port odor delivery (or in earlier stages, their entry into the side port) and the reward outcome, the correctly chosen reward port illuminated and a tone played for 50 ms to indicate whether that trial would be rewarded. This then gave mice 2 s at full delay to return to the reward port and collect water. A 500-Hz tone indicated a rewarded trial, while a 2,000-Hz tone indicated an unrewarded trial.

Task with four information- and water-predicting CS odors at the center port. Five mice with completed surgery for OFC imaging that had been previously trained on the information seeking task and had strong information preference were trained on this additional task (Fig. 3d). First, mice were trained to follow the 'high water value' odor to one side port and receive 8 × 4-µl drops of water and the 'low water value' odor to the other side to receive 2 × 4-µl drops of water. The side that had previously been the preferred information side was assigned as the small water side. One side port was covered and mice performed blocks of trials on one side, then the other. Then these two large and small water trial types were pseudo-randomly interleaved with all ports uncovered. Owing to limitations in the olfactometer, which could only provide four odors at the center port, the odor that had previously indicated free choice trials became the 'small water' odor and the fourth odor that had not previously been used was the

'large water' odor. Mice performed seven to ten training sessions in this stage. Mice then performed one to three sessions of interleaved forced information and forced no information trials as they had learned earlier in the main task version. Mice then performed the full version of this task with information, no information, large water and small water trials pseudo-randomly interleaved in blocks of eight to ensure adequate exposure to all trial types. Mice performed six sessions with the sides in the initial configuration followed by six sessions with the side identities reversed. Information and low water value were assigned to the same side port, while no information and high water value were assigned to the other.

Licks

Licks were recorded in initial behavioral sessions ($N = 14$ mice) using capacitance sensors (Phidgets, 1129_1B) at each port's lick spout.

Stereotactic surgery

Mice were anesthetized with ketamine (100 mg kg^{-1}) and xylazine (10 mg kg^{-1}) through intraperitoneal injection and received analgesia via buprenorphine sustained-release subcutaneous injection (0.75 mg kg^{-1}) and carprofen (3 mg kg^{-1}), had fur shaved from their head and then were placed in a stereotactic frame. Body temperature was maintained using a heating pad attached to a temperature controller. For lens implantation experiments, a 1.1–1.5-mm round craniotomy centered on the implantation coordinates was made using a dental drill. The dura was removed and <0.1 mm of tissue aspirated, and 0.3 µl GCaMP6f virus (AAV1.CaMK2a.GCaMP6f.WPRE. bGHpA, 3.35×10^{12} vG ml^{-1}, Inscopix) was injected into lateral OFC (medial-lateral (ML), 1.0; anterior-posterior (AP), 2.4; dorsal-ventral (DV), 2.45 mm from Bregma) at ~50 nl min^{-1} using a pulled micropipette. After allowing the virus to diffuse undisturbed for 5 min, the needle was removed and a 0.5-mm or 1-mm diameter and 4.0-mm length microendoscope GRIN lens with integrated baseplate (Inscopix) was then inserted at a depth just above the injection site and centered over it (ML, 1.0; AP, 2.4; DV, 2.4 mm from Bregma). The combined lens and microscope baseplate assembly (Inscopix) was secured to the skull using Metabond (Parkell) and further secured and covered with black dental cement (Ortho Jet). Mice recovered for at least 1 week before the beginning of water restriction and behavioral training.

Histology

Mice were euthanized after anesthesia with ketamine/xylazine by perfusion with 4% paraformaldehyde. Brain tissue was removed for 24 h fixation, and coronal sections (120 µm) were cut on a vibratome (Leica). The sections were incubated with far-red neurotrace (640/660, Thermo Fisher Scientific) to label neuronal cell bodies. Images were collected using a Zeiss LSM-710 confocal microscope system. Histology was performed to confirm locations of implanted lenses, as well as expression levels for GCaMP using native fluorescence.

Imaging experiments

Seven mice were imaged throughout the course of training and testing in the main task, including during 10-s and 1-s delay sessions (Supplementary Tables 3–7). Five additional mice were imaged throughout learning and performance of the four-odor center port information and water prediction task (Supplementary Table 8). Recordings of GCaMP activity were made using Inscopix miniaturized microscopes (nVista3.0) with commutators used in passive mode, with uncompressed videos saved using the Inscopix system. Before being placed in the behavior chamber, awake mice had the miniature microscope (Inscopix) attached securely to their skull baseplate. Neural activity was then recorded throughout the behavior session (50–100 min) and the microscope was removed and the baseplate cover reattached. Images were recorded with the lowest possible LED illumination to visualize calcium transients with settings largely preserved from session-to-session within each animal. Generally, LED power was set between 0.3 and 1 mW, with most animals remaining <0.7 mW. The z focus of the microscope was adjusted rarely to maintain the same field of view based on landmarks such as blood vessels.

Quantification and statistical analysis

No statistical method was used to predetermine sample sizes. All mice that completed training during water restriction with adequate weight maintained and that displayed the expected differences in reward port occupancy based on the predicted water reward were included in preference testing and shown in Fig. 1b–e. Less than 15% of mice failed to learn the task by this criterion. Mice that displayed information preference on both the left and the right side were used for water and delay titration and imaging experiments given that these experiments were designed to test the effect of increases in information cost and decreases in information value on information preference. Both male and female mice were used, information preference data are reported disaggregated, and no difference was observed. Blinding of experimenters to conditions was not applicable. Information side and odors were pseudo-randomly assigned across animals.

Statistical tests are indicated in the text and/or figure legends. Nonparametric tests were used unless otherwise described. Tests are two tailed unless otherwise noted. Exact P values are given, except for when below the level of computer precision or in permutation tests, when the observed value exceeded all permutations.

Behavior analysis

Behavior was analyzed using custom MATLAB scripts. Mice performed approximately 150 trials per session. We examined information preference on free choice trials across all of the preference testing sessions ('overall preference'; Fig. 1c) or in the last 200 free choice trials prior to the first side reversal and the last 200 trials after reversal before either ending preference testing, reversing the sides again or progressing to delay or reward amount manipulations. For most animals, these 200 trials occurred in the last 3 days before and after reversal, since mice performed around 50–60 choice trials per session. Extended Data Fig. 1j shows pre-reversal preference in these 200 choice trials and Fig. 1d shows preference before and after reversal. Since choice preference is the probability of the binary outcome of choosing information or no information, we used MATLAB's binofit function to estimate the information choice probability, P(info), and 95% CIs for each animal. We then tested whether the means of these values across animals were different from 50% (indifference) using two-sided sign rank tests (MATLAB signrank). We fit a generalized linear regression model to compute coefficients for the correlation of side and information with choice for each animal using MATLAB's glmfit function for binomial data with the default 'logit' link function (Extended Data Fig. 1l). These coefficients provide the 'log odds' influence of side and information on choice.

We also estimated the probability of correct choice on forced trials using binofit and report data across animals in the same way as preference. For reward rate, licks and probability of poking in nose ports, we report the mean across sessions per animal and computed the population mean and standard error. Reaction time is the time elapsed from the go cue until the first entry of the correctly chosen side port and is reported per-trial by trial type. Reward rate is calculated as the mean water amount received per minute of correct trials. The probability in port is shown as either the mean across the delay between the end of the side port odor stimulus and the reward outcome or the mean across the first 1 s after the end of the side port odor stimulus. On plots showing the full trial duration (Fig. 1h and Extended Data Fig. 2d), the trial is binned into 50-ms increments to compute the probability of being in a particular port. In contrast to the correlation we identified between information preference and reaction time (Extended Data Fig. 1n), we did not detect correlations between information preference and time

spent in the information versus no information port, licking before receipt of the side port odor or licking following information odor A (water) and information odor B (no water).

Unless otherwise indicated, behavioral data are from the last three sessions before the first side reversal. Before pooling data across sessions, we confirmed that there were not significant cross-session differences using a nonparametric within-subjects design (Friedman's ANOVA with Tukey–Kramer correction for multiple comparison).

Behavioral models

Cognitive decision models, fit to single trial level-choice data, have been used in neuroscience and behavioral economics for decades to provide evidence that a specific type of computation may be underlying choice trends seen in a given dataset[71]. The two main questions we sought to answer with decision model frameworks here were (1) 'why do information-preferring mice not always choose information?' and (2) 'can the observed experimental behavioral trends be explained by a model that uses separate but interacting reinforcement learning (RL) machinery for processing traditional water rewards and intrinsic information rewards?'. We hypothesized that there is an interaction between RL-like computations of information value and water value following recent literature[21] and used a list of relevant models of increasing complexity to test this hypothesis.

In decision model literature, there are a large variety of RL-related models, often becoming quite complex, which risks overparametrization and over-fitting if the number of agents fit and task complexity do not scale with the model complexity[72,73]. Thus, for the purposes and constraints of this study, we chose to use the simplest implementation of RL computations, the Rescorla–Wagner model, following similar recent related work in human models[40]. The models tested are outlined below and incrementally built up to the full model that contains the minimal necessary components to explain both the water-tuning and delay-tuning experiments (Fig. 1j,l and Extended Data Fig. 3). The MATLAB package fitPsycheCurveWH was used to fit a psychometric curve to each mouse's real choices as well as the predicted choices from each of the models tested, using the best parameter initializations from a grid search.

First, all models tested transform a decision variable DV term, which summarizes the core computation, into a sigmoid-transformed binary choice probability $P(t)_{\text{info}}$, here the probability of choosing information at trial t

$$P(t)_{\text{info}} = \frac{1}{1 + e^{[-DV(t)]}} \tag{1}$$

The term $P(t)_{\text{info}}$ is optimized through a negative log likelihood minimization

$$\text{NLL} = -\sum_{t=1}^{n\text{Trials}} \{\log(P(t)_{\text{info}})\, C(t)_{\text{info}} + \log(1 - P(t)_{\text{info}})(1 - C(t)_{\text{info}})\} \tag{2}$$

where is $C(t)_{\text{info}} = 1$ for an information choice and 0 for a noninformation choice. Models were each run with 16 initializations of different starting parameter values and numerically solved using the fminsearchbnd function in MATLAB using a grid search of parameter windows. The nature of DV(t) changes in each model, as summarized below

RL water model

$$\text{DV}(t) = \frac{1}{\sigma}\{\beta \Delta Q(t) + \varepsilon\} \tag{3}$$

The time-independent fit parameters are σ, the normalization constant (inverse temperature), β, a relative weight factor for the traditional Rescorla–Wagner RL term of water $\Delta Q(t)$ and ε, a bias term, which allows for a flat baseline tendency toward or away from choosing information that the water term is weighted against. The time-dependent term $\Delta Q(t)$ is defined as the difference of the value functions for the information and no-information sides of the task as usual in binary choice tasks

$$\Delta Q(t) = Q(t)_{\text{info}} - Q(t)_{\text{no-info}} \tag{4}$$

Each $Q(t)_i$ for i = info, no info is defined according to the Rescorla–Wagner equation with learning rate α_1 and prediction error $\delta(t)$ when choice i is chosen

$$Q(t)_i = Q(t-1)_i + \alpha_1 \delta(t)_i \tag{5}$$

$$\delta(t)_i = \text{Reward}\,(t-1)_i - Q(t-1)_i \tag{6}$$

When a choice is not chosen, with unchosen choice j, then $Q(t)_j = Q(t-1)_j$.

The next model tested contains only information-related terms with a new Rescorla–Wagner term $S(t)$ for information value with information prediction error $\theta(t)$ and learning rate α_2, following analogous logic to recent nontraditional RL equations such as choice prediction errors[74]

λ-RLinfo model

$$\begin{aligned} \text{DV}(t) &= \tfrac{1}{\sigma}\{S(t) + \varepsilon\} \\ S(t) &= S(t-1) + \alpha_2 \theta(t) \\ \theta(t) &= \left\{\left(\tfrac{\text{Delay}(t-1)}{10\text{s}}\right)^{\lambda} - S(t-1)\right\} \text{if info is chosen} \\ \theta(t) &= \{0 - S(t-1)\} \text{if noinfo is chosen} \end{aligned} \tag{7}$$

Thus, information's 'value' is $\left(\frac{10\text{s}}{10\text{s}}\right)^{\lambda} = 1$ for the maximum delay of 10 s, but then is exponentially discounted as delay decreases, following the strong tendency observed in the mice data. When the mice do not choose information, they receive no information value and thus the info-reward is set to zero.

The next model tries to remove the λ decay exponent, but combine the RLwater term with the RLinfo term simplified to have $\lambda = 0$, so that information value = 1 on information choices regardless of delay length.

RLwater + RLinfo model

$$\text{DV}(t) = \frac{1}{\sigma}\{\beta \Delta Q(t) + S(t)_{\lambda=0} + \varepsilon\} \tag{8}$$

Then, the full model combining both water value and exponential delay-modulated information value computations is defined below, conceptually motivated by recent work finding both types of value are processed in an interacting way[21].

RLwater + λ-RLinfo model:

$$\text{DV}(t) = \frac{1}{\sigma}\{\beta \Delta Q(t) + S(t) + \varepsilon\} \tag{9}$$

As an alternative to exponential modulation of the information value by the delay length, we also tested a hyperbolic variant of equation (7), replacing $\left(\frac{\text{Delay}(t-1)}{10\text{s}}\right)^{\lambda}$ with a hyperbolic term $0.5(1 - \kappa \frac{\text{Delay}(t-1)}{10\text{s}})^{-1}$

RLwater + λ-RLinfo model (hyperbolic)

$$\text{DV}(t) = \frac{1}{\sigma}\{\beta \Delta Q(t) + S(t)_{\kappa} + \varepsilon\} \tag{10}$$

Last, as a conceptually alternative decision model, we made a weighted win-stay lose-shift (WS-LS) model, that regressed the past trial information and reward conditions to predict the current choice

WS-LS model

$$\mathrm{DV}(t) = \frac{1}{\sigma}\{\beta_1 \mathrm{InfoRew}(t-1) + \beta_2 \mathrm{NoInfoRew}(t-1) + \beta_3 \mathrm{InfoNoRew}(t-1) + \beta_4 \mathrm{NoInfoNoRew}(t-1) + \varepsilon\} \quad (11)$$

Each β_i condition variable is either 0 or 1. For example, Info No Rew = 1 if the past trial was an unrewarded information choice (either forced or choice), but 0 otherwise.

The total number of mice fit was $N = 10$ for all models, but for 4/10 mice only the water tuning data was fit, not the delay-tuning data since those mice did not perform delay-tuned task variants. These mice have had their λ discount exponent removed as shown in Supplementary Table 9 of fit parameters. Then 4/10 mice did not have water tuning data fit. These mice have all fit parameters in Supplementary Table 9. To show the data were not overfit, each model was fit five times with different randomized 67% train versus 33% test splits per model for cross-validation (Supplementary Table 10). Mean and standard deviation of normalized AIC and accuracy are shown in the table across the five runs.

To see how much each RL component improved the full model fit, the average Akaike information criterion (AIC) was calculated according to the standard equation for each model, with k as the number of free parameters[75]

$$\mathrm{AIC} = 2k + 2\mathrm{NLL} \quad (12)$$

The full RLwater + λ-RLinfo model is shown in Fig. 1. The auxiliary models are presented in Extended Data Fig. 3. It is visually clear that only the RLwater + λ-RLinfo can simultaneously capture the important trends from the data in both water tuning and delay-tuning experiments. Future work seeking to do more advanced decision modeling with further corrections to the Rescorla–Wagner formulation should increase the sample size and tune a wider range of experimental conditions, but the current models implemented show that the minimally simple RL formulation that accounts for both water value and information value is able to explain the full range of experimental conditions tested here. As a caveat, we do not claim our fitted parameters are unique or will work for all future studies, a common issue in cognitive decision models because model parameter magnitudes and scaling are not independent and thus degenerate solutions probably exist[71,72]. However, this well-known issue does not undermine the finding that the minimal two-value-type RL model machinery performs well in our context.

Imaging data processing

Raw video data were spatially downsampled at 4× and saved as Tiff files using the Inscopix Python API. We used the NormCorre rigid motion algorithm[76] to both remove movement artifacts from imaging videos and to align the field of view across sessions to facilitate cell registration. We motion corrected videos filtered to reveal more stationary landmarks such as blood vessels and then applied the computed X–Y shifts to the original videos. To filter videos, we took a difference of Gaussians approach to extract potential stationary features smaller than cell diameter from the larger background fluctuation. We applied a Gaussian filter (Matlab imgaussfilt) with a radius of 2 to our downsampled 200 × 320 pixel images and subtracted pixel values of the images separately filtered with a larger radius (MATLAB imgaussfilt radius 6). We then set a threshold value of 4 and set all pixel values less than this threshold to its value. This resulted in a filtered video with mostly black background and light-to-white landmarks on which we performed motion correction and generated a mean template image.

Motion correction was performed within each session using the NormCorre algorithm using the following parameters: 'bin_width' 500, 'init_batch' 1,000, 'max_shift' 10, 'iter' 2. We then used NormCorre to align each session's video frame-by-frame to the filtered template from a central 'anchor' session for each animal (typically the final day of preference testing before the first side reversal). The alignment of the template field of view from each session was manually inspected to ensure accurate registration across sessions. Cell location footprints and activity were then extracted using the MATLAB implementation of CNMF-E[77] as follows.

CNMF-E default parameters were used, except that min_corr and min_pnr were adjusted for each animal to maximize cells identified during the initialized step of the algorithm (min_corr range 0.7–0.8, min_pnr 8–10) and gSig = 3, gSiz = 11. For initialization, min_pixel was set to 25 and for identification of cells in the residual after background subtraction, min_corr_res = 0.8 and min_pnr_res = 9. Following two iterations of CNMF-E's cell footprint and calcium activity extraction, we applied several additional filters to remove false positives, taken from the incorporation of the CNMF-E algorithm into the Caiman Python implementation[78]. We set thresholds for temporal sparseness, minimum peak-to-noise and a constant baseline of activity. We first removed cells with temporal sparsity <0.003.

$$\begin{aligned}&\text{Temporal sparsity}\\&= \mathrm{sqrt}(\mathrm{sum}(\mathrm{neuron.C\_raw.}\hat{}\,2, 2))./\mathrm{sum}(\mathrm{abs}(\mathrm{neuron.C\_raw}), 2)\end{aligned} \quad (13)$$

We then removed cells with peak_to_noise_ratio <8.5

$$\mathrm{PNR} = \max(\mathrm{neuron.C}, [], 2)./\mathrm{std}(\mathrm{neuron.C\_raw} - \mathrm{neuron.C}, 0, 2) \quad (14)$$

Finally, we removed cells in which CNMF-E's detrending of the calcium fluorescence across the session was ineffective and that had large differences in the baseline fluorescence between the beginning and end of the session. We computed the difference from baseline by taking the difference in mean activity between the first and last 10% of the session frames and removed cells for which this absolute value was greater than 3.

$$\begin{aligned}&\mathrm{difference\_from\_baseline} = \mathrm{mean}(\mathrm{neuron.}\\&\mathrm{C\_raw}(:, 1 : \mathrm{round}(0.1{*}\mathrm{size}(\mathrm{neuron.C\_raw}, 2))),\\&2) - \mathrm{mean}(\mathrm{neuron.C\_raw}(:, \mathrm{end} - \mathrm{round}\\&(0.1{*}\mathrm{size}(\mathrm{neuron.C\_raw}, 2)) : \mathrm{end}), 2)\end{aligned} \quad (15)$$

We then visually inspected each cell using CNMF-E's viewNeurons method to ensure appropriate neuron-like shape and calcium transients and removed false positive cell identifications.

Using this procedure, we were able to register cell spatial footprints across sessions several weeks apart, over the entire months-long course of training, for up to four sessions simultaneously using the register_multisession function from the MATLAB implementation of CaImAn[78]. We used the default parameters for register_multisession, with the exception of setting the threshold for turning spatial components into binary masks, options.dist_maxthr = 0.22, and the threshold for setting a distance to infinity, options.dist_thr = 0.6. Cell registration fidelity between individual sessions was visually inspected using the register_ROIS method for maximum overlap and false positives to appropriately set parameters. For 4/5 mice imaged in the four center port odor information and water value prediction task, a newer algorithm, SCOUT, was used to register cells. SCOUT registration of cells used the default parameters[79].

Analysis of neural activity

We used the calcium signal, C, output by CNMF-E that is smoothed with a kernel based on the time course of GCaMP6f signal decay as the calcium activity, a proxy reflecting neural spiking activity, of each cell across each session. As CNMF-E subtracts the background signal from each imaged frame individually, the output activity, C, may be considered a scaled version of the change in fluorescence over background

($\Delta F/F$) at each frame. Moreover, given this background subtraction, this signal is already normalized[77]. We therefore analyzed and report raw 'calcium activity'. We also tested a standard z-score normalization procedure subtracting each cell's mean across each session and dividing by the standard deviation, and this did not qualitatively affect the results.

Neural activity in each session was aligned to behavioral events using DAQ timestamps, and we analyzed neural activity across all mice considering cells across animals as a single pool for single-cell analyses, except where otherwise noted. Our CEBRA model simultaneously fit across animals using all cells, not just those registered day to day, with the same qualitative findings about information and water value encoding supports pooling cells across animals. The main dataset (Supplementary Table 3) consisted of cells registered across four sessions surrounding a side reversal such that there were two sessions with information on each side (left and right), with 56–216 cells per animal across seven animals (N = 1,138 total neurons). Datasets for delay comparisons (10 s versus 1 s; Supplementary Tables 5–7) and learning (Supplementary Table 4) also consisted of four sessions per animal across six and seven animals, respectively, with similar numbers of cells per animal (N = 992 total delay neurons, 788 total learning neurons). Data for mice imaged in the four-odor center port information and water value prediction task involved cells registered across four sessions surrounding a left–right side reversal, with 964 cells from five animals (Supplementary Table 8).

All analyses of neural activity used correct forced trials, except those of Fig. 3c,h and Extended Data Fig. 6a–d,g, which used choice trials. Analyses of the main dataset and four CS center odor task balanced left and right side trials by matching sessions across side reversal thus approximately equalizing the number of correct forced information and no information trials on each side given the pseudo-random block trial structure for the calculation of coding indices (below) and mean activity. Decoding analyses precisely balanced trials across sides (details below). Analyses across task learning and information value manipulations necessarily used data with information on a single side.

We computed indices of cross-validated differential activity to analyze OFC neurons' encoding of task variables (coding index). For each pair of conditions (for example, information and no information) within each neuron, we balanced (cross-validated) the direction of the difference in activity (that is, sign). We multiplied the mean difference in activity between the two conditions for one arbitrary half of the trials (for example, even-numbered trials) by the sign of the mean difference on the other half of the trials (for example, odd-numbered trials) and vice versa, and then took the mean value of these two split halves as the coding index for that cell

$$\begin{aligned}\text{coding index} = (&\text{sign}(\text{activity difference in OddTrials}) \times \\ &\text{activity difference in EvenTrials} + \\ &\text{sign}(\text{activitydifference in EvenTrials}) \\ &\times \text{activitydifference in OddTrials}) * 0.5\end{aligned} \tag{16}$$

This procedure is similar to taking the absolute value of the difference in activity but instead creates an index of differential activity centered at zero in the absence of consistently greater activity in a particular condition. We then averaged these indices to find the coding index across the population.

We computed the coding indices across the full trial time course at each imaged frame, beginning at the onset of center port odor on the mouse's center port entry that successfully initiated the trial. Mice sometimes entered the center port and received a partial odor stimulus prior to successfully initiating a trial by remaining in the port through the completion of the go cue tone, which may have meant that OFC responded differently at the animal's first and subsequent center port odor presentations. Thus, we computed full-trial coding indices surrounding the odor presentation at successful trial initiation, from which the remaining trial events proceeded.

To analyze neural responses and identify CS and US value representations at specific trial epochs, we examined coding indices in a 1-s window following each trial event: the first center port odor presentation, the side port odor presentation and the reward outcome. We determined the 1-s post-event activity window by observing the raw odor responses and peak differential activity around each event in our task. We also determined the time course of odor stimulus delivery in the nosepoke ports using a photoionization detector (Aurora Scientific, 200b miniPID). Although we observed small differences in the timing of odor availability, on average odor was first detectable 0.075 s after odor valves were open and peaked at 250 ms after valve opening. The neural responses we observed peaked within 1 s of odor onset. We have therefore used a window of 0.2–1.2 s after the timing of events recorded by our Bpod system (odor and water valve opening), and a comparable window 1.2–0.2 s before events, to analyze neural responses. For plot visualizations, we have indicated odor onsets 0.075 s after the opening of the odor valves in the olfactometer.

To determine whether cells, and the OFC population on average, encoded differential activity between two conditions as computed in our coding index in a task epoch, we took a bootstrapping approach. We compared the difference in the mean coding index in the 1 s window after an event to the mean index in the 1 s window before it to account for the fact that activity continuously varied throughout the task and, in particular, was often already elevated just before the side port odor delivery. Thus, for a given set of conditions (for example, information and no information), we shuffled trials between the two conditions 1,000 times. For each shuffle, we determined the difference between the mean coding index in the 1-s window after the trial event and the mean coding index in the 1-s window before the trial event. We then determined the percentage of these shuffled values that were less than the observed increase in differential activity to estimate the statistical likelihood of the observed difference (P value). We defined a cell as contributing to a representation or encoding a difference between conditions if the observed coding index difference was greater than that of at least 5% of shuffled data. Similarly, we defined that the OFC population encodes a difference between conditions if the mean population coding index difference around an event was greater than 95% of the shuffled values. Extended Data Fig. 5b–e shows the event-specific coding indices we computed in addition to the full trial information and water coding indices.

We performed a shuffling procedure to evaluate the statistical significance of the different correlation values for the data in Fig. 3h,i. Under the null hypothesis that these two datasets come from a common underlying distribution, we combined all the data points in these two figures and randomly assigned them to two groups, with the number of points in each group matching the numbers in the figures. We then computed the ratio of correlation coefficients for these two random groups. We repeated this for 100,000 random shuffles and report the fraction of shuffles for which the ratio was greater than or equal to that of the data.

Cells with significant conditional responses to task events (responding cells)

Cells were identified as responding to an event in a task condition using a rank-sum test to determine if their activity in the post-event 1-s period (as above) in that condition was different from activity in the pre-event 1-s period in that condition, which we considered the baseline activity for that event. To accommodate baseline activity that was already elevated due to earlier trial events given the close proximity in time of the center and side port odors, we determined the maximum activity for each cell on each trial in the pre-event period and fit an exponential decay function based on GCaMP6f fluorescence (λ = 4) to determine its predicted activity in the post-stimulus period. If the absolute value of difference between the mean of that predicted

activity in the post-event period and the mean of the observed activity in the post-event period on that trial was greater than 0.2, the GCaMP fluorescence-predicted activity in the post-event period was used as the baseline. If not, the pre-event activity served as the baseline. Cells with significant responses were then identified as those in that condition with mean activity in the post-event period significantly greater than baseline using a rank-sum test and with the value of that difference greater than 0.1. This procedure offers a conservative identification of responding cells to prevent false positives. Using a more standard procedure with a rank-sum test on mean activity before and after the event falsely identified many cells with delayed responses to the center port odor whose activity then diminished as expected for calcium signals at the same time as the side port odor delivery as 'responding' to the side port odor. We therefore used the above approach to more conservatively identify cells with activity changes due to the side port odor.

Mean activity

For plots showing population mean activity, each cell's mean activity on the indicated trial type was calculated, its mean activity within the 1-s pre-event window was subtracted and then all cells' mean activities were averaged. Single-cell plots are shown with the mean activity in the 1-s pre-event window subtracted. To test whether the population mean responses to center port odors changed across delay changes and learning (Extended Data Fig. 8a,k), we compared the mean activity in the 1-s window after the center port odor across all trials between the two conditions, using a rank-sum test for significance.

Heat maps

Population calcium activity and coding index heat map plots display the mean activity or coding index for each cell across trials in each condition. Heat maps of mean calcium activity, and not those of differential activity using coding indices or activity differences, have the cell's mean activity in that condition across the pre-event 1-s period subtracted for better visualization. Plots within panels are all sorted by the indicated activity such that a single cell can be read across the entire heat map.

Decoding

Linear classifiers based on support vector machine architecture were used to decode trial types using the Decodanda Python package (https://github.com/lposani/decodanda)[80]. Decodanda uses the Python package scikit-learn to implement support vector machines. Classification was performed on 200-ms bins of neural data, with calcium activity averaged for each cell on each trial within each bin or, for overall mean classification accuracy, on calcium activity averaged for each cell on each trial within the 1-s window following the center odor stimulus onset (post-event period). For decoding accuracy across bins of time in trials, analysis was performed separately for each time bin. Decoding performance was computed using 20-fold cross-validation, in which trials for each animal were split into samples for training (75% of trials) and testing (25%) sets at each fold. Decoding accuracy was taken as the mean across the 20 cross-validation folds. Trial samples were balanced across both information or water value conditions and left–right side across side reversals to eliminate confounding between possible side location and value encoding. Trials were either sampled from imaging sessions within a single animal or by pooling across animals. Pseudo-populations of cellular activity were generated by sampling an equal number of trials ($N = 200$) of each combination of conditions from each animal. For example, to decode information versus no information trials, in each cross-validation fold, each animal's information left, information right, no information left and no information right trials were split into testing and training fractions. Then, 200 samples were taken from each set of conditions for training. These data are then pooled across animals. For decoding of free choice trials (information choice versus no information choice), only data from four of seven mice were used because the other three animals had fewer than four no information choice trials on one side due to high information preference. Accuracies were compared to the decoding accuracy obtained from a null model computed by randomly shuffling the labels of trials. For each decoding test, ten null model iterations were performed, and statistical significance of the performance accuracy of data decoding was determined by the one-tailed z score compared to the distribution of null model accuracies.

We determined the coding importance, w_i^x, of each cell for each classifier, following the method employed in ref. 80. For each variable, X, for each cell i, we computed the absolute value of the average decoding weight normalized by the standard deviation across validation folds, where n is the cross-validation fold

$$w_i^x := \left| \frac{E\left[w_{i,n}^x\right]_n}{\sigma E\left[w_{i,n}^x\right]_n} \right|$$

We then computed the Pearson correlation between these weights for the information versus no information and high versus low water value classifiers. We also computed the correlation between these weights for the information forced versus no information forced and information choice versus no information forced classifiers.

Principal component analysis to identify information–no information axis in population activity space

To compute an axis along the information–no information dimension in population activity space, we calculated the difference between the mean activity on correct information forced and the mean on correct no information forced trials for each cell following the center port odor presentation (0–0.8 s after odor valve opening) in our main dataset with two sessions with information on the left and two on the right side. We then computed the principal components of that population activity difference (MATLAB function svd). The first component captured >80% of the variance in this activity computed from the variance of the projection of the information and no information trial activity onto the first component divided by the total variance of activity on information and no information trials. We therefore projected the population activity in each trial, and the mean within each condition (information and no information), onto the first principal component for visualization.

CEBRA modeling

We used CEBRA to better understand how a complex task such as ours is represented at the neural level. The complexity of our task, together with the possibility that the OFC, as a frontal region, contains neural representations that are more compressed and processed compared to other regions, suggested that neural task representations are more likely to have arisen from the nonlinear combination of neural signals[33,36]. A nonlinear latent variable model such as CEBRA, unlike principal component analysis, for example, reduces the chance that an analysis is fitting task-irrelevant noise or missing important nonlinear signals that are crucial to accurately capture how a task is encoded at the population level.

More specifically, we used CEBRA to obtain low-dimensional task embeddings by jointly fitting neural data and task-relevant behavioral variables in a time-dependent manner. We generated time-stamped labels expressing task structure and mouse behavior, as further specified below, and fitted these together with the neural data by minimizing an InfoNCE contrastive loss objective[53]. We fit the model to the entire cohort of animals at once, such that contrastive samples were chosen from across all animals. We thus obtained latent embeddings that were informative and consistent across animals. We examined the geometry of the information and water value representations in the embeddings and measured the differences between these two representations over the course of each trial. We confirmed that the embeddings were informative by decoding task-relevant variables and comparing results to shuffled versions that scrambled the association of particular labels with the recordings.

We fit CEBRA models with the following specifications: model architecture = 'offset1-model', batch size = 1,024, distance = 'cosine', conditional = 'time_delta', temperature = 'auto', learning rate = 0.001, max iterations = 5,000, output dimension = 3, number hidden units = 100. We arrived at these settings by fitting CEBRA models on the data from three mice and picking the settings that achieved the lowest overall InfoNCE[81] loss value after 10,000 iterations; during this process we observed that only half the iterations were necessary for the loss to converge so we set max iterations to 5,000 to minimize compute.

We fit two types of models which we refer to as full and delay. The full model is fit on data with a long delay (t_d_l = 10 s) between the side port odor and reward delivery, while the delay model is fit on data with both short (t_d_s = 1 s) and long delay (t_d_l = 10 s) and is aimed at embedding the two delay types in a joint space for comparison.

The full model was fit on six mice (JB432, JB426, JB434, JB413, JB424 and JB425) with cell and trial counts as specified below (Supplementary Table 11). Importantly, we employed a multisession setup in which each session with its unique dimensionality was added into the fitting process accompanied by shared context labels (Supplementary Table 13), which allowed CEBRA to learn a shared embedding space for signals from all sessions (across all mice). We used sessions from our main dataset balanced before and after information side reversal, such that each mouse was fit with two sessions with information on each side (left/right). To achieve an unbiased representation across all conditions, we equilibrated the number of trials across conditions such that there were equal numbers of trials across the four conditions resulting from the interaction of 'reward versus no reward' and 'information versus no information'. For the full model, the number of time points per trial is fixed at *n*_time = 320 time points per trial throughout, ranging from the initiation of the last (if multiple) presentation of the center port odor all the way until after reward delivery.

The delay model was fit on six mice (JB432, JB433, JB434, JB426, JB424 and JB425) with cell and trial counts (Supplementary Table 12) and label types (Supplementary Table 13) with *n*_time = 113, as specified below. To make the two delay types (short and long delay) comparable, with identical context labels across sessions allowing sessions with variable cell counts to be fitted together in one model, we excerpted the outcome period in the long delay trials and concatenated it after the first ~1 s of the 10-s delay period (omitting most of the longer delay) thus making the overall duration of short and long delay trials the same. These sessions do not include a reversal of the information port location. As before, to achieve an unbiased representation across all conditions, we equilibrated the number of trials across conditions such that there were equal numbers of trials across the four conditions resulting from the interaction of 'reward versus no reward' and 'information versus no information'; in case that resulted in less than one trial per condition, we equilibrated instead by 'information versus no information' only (session marked with * in Supplementary Table 12).

Unlike the full model, we matched cells across all recording sessions for a particular mouse before fitting the delay model (hence the matching cell counts in Supplementary Table 13). We then combined all of a mouse's recording sessions into a single array and fitted the recordings and labels (Supplementary Table 11) with CEBRA in a single-session setup. This allowed us to derive a common embedding space across both delay types.

We fit all CEBRA models on the neural data (as defined above) together with the specified label types (Supplementary Table 13). Labels are zero everywhere except between the start and end frame where they are set to nonzero values depending on label type.

We obtained the decoding performance for the CEBRA embeddings. We divided the data from each animal and session separately into a train and a test set such that data from each animal and session was present in both sets, with 40% of the data being assigned to the test set. We obtained a CEBRA fit on the train set with the parameters described above and then projected the train set recordings into the embedding space. We thus obtained three-dimensional embeddings for every trial in the train set and used these trajectories to train a *k*-nearest neighbors classifier with a cosine-distance metric and $k = 20$. We fitted separate classifiers for each label type to be decoded. We then used these classifiers to predict a given label type at each point in a trial for all the recordings in the test set. To quantify performance, we calculated the balanced accuracy score across a bin of five samples with a step size of one, and averaged results across sessions, animals and runs. The results we report are averaged across five runs, meaning five separate CEBRA fits with different random seeds. We calculated the 95% CI for the decoded accuracy results across the six animals, accounting for dependent measurements across sessions[82].

We also fit label-level controls. There were four different label-level control types: 'shuffled trials all labels', 'shuffled max all labels', 'shuffled info label' and 'shuffled reward label'. For the 'shuffled trials all labels' condition, we randomly scrambled the assignment of trials to their original time-varying labels, for all the label types, but left the relation between labels and the time they were assigned in a trial (Supplementary Table 13) intact. For the 'shuffled max all labels' condition, we randomly scrambled both the trial and the time affiliation of a given label, for all label types, thus resulting in the maximum amount of signal scrambling. For the 'shuffled info label' condition, we only scrambled the trial-label assignment for the 'info versus no info' label type (Supplementary Table 13), leaving all others intact. For the 'shuffled reward label' condition, we only scrambled the trial-label assignment for the 'rewarded versus unrewarded' label (Supplementary Table 13), leaving all others intact. Otherwise, controls were fitted identically to the full model. Results are again reported as an average across five runs, using different random seeds to achieve the train/test allocation (Extended Data Fig. 9).

In addition, we fit cell-level controls. There were two different cell-level control types, 60% and 20%, with the percentage number indicating how much of the original population of recorded cells was used (Supplementary Tables 11 and 12). So, for instance, in the 60% condition, only 60% of the cells in a given session were randomly picked to be included in the fit. This was also repeated across five runs, using five different random seeds to subsample the cells. Results are reported averaged across sessions, animals and runs.

Finally, we obtained the distance between individual trajectories in the embedding space. For that we projected all the recordings into the embedding space obtained by the full CEBRA model fit. To determine the distance in neural population space between task embeddings in the various experimental conditions ('info', 'no info', ...), the Euclidean distance was calculated between all possible trial pairs. Cross-session and cross-animal first and second moments were calculated by inverse-variance weighting. Averaged cross-session variances and cross-animal variance were added to obtain the final 95% CI.

Reporting summary

Further information on research design is available in the Nature Portfolio Reporting Summary linked to this article.

Data availability

The behavioral and neural data generated and analyzed in this study are available via Zenodo at https://doi.org/10.5281/zenodo.20450673 (ref. 83) (behavior), https://doi.org/10.5281/zenodo.20452041 (ref. 84) (main imaging data), https://doi.org/10.5281/zenodo.20466860 (ref. 85) (imaging data, learning), https://doi.org/10.5281/zenodo.20470580 (ref. 86) (imaging data, delay sessions), https://doi.org/10.5281/zenodo.20470622 (ref. 87) (task with four center port odors, information versus water value), https://doi.org/10.5281/zenodo.20477351 (ref. 88) (imaging files JB413, JB424, JB425 and JB426), https://doi.org/10.5281/zenodo.20479276 (ref. 89) (imaging files JB432, JB433, JB434, JB483 and JB484) and https://doi.org/10.5281/zenodo.20480778

(ref. 90) (imaging files JB506, JB507, JB509). Preprocessed and motion corrected calcium imaging video files are available via Figshare at https://doi.org/10.25452/figshare.plus.32582997 (ref. 91). Owing to their large size, the raw calcium imaging video files are available from the corresponding author upon reasonable request. Source data are provided with this paper.

Code availability

The code used to generate and analyze the data and create the figures is available via GitHub at https://github.com/jjbussell/Bussell2026InfoValue.

References

71. Daw, N. D. Trial-by-trial data analysis using computational models (Tutorial Review). In *Decision Making, Affect, and Learning: Attention and Performance XXIII* (eds Delgado, M. R., Phelps, E. A. & Robbins, T. W.) (Oxford Univ. Press, 2011).
72. Eckstein, M. K., Wilbrecht, L. & Collins, A. G. What do reinforcement learning models measure? Interpreting model parameters in cognition and neuroscience. *Curr. Opin. Behav. Sci.* **41**, 128–137 (2021).
73. Wilson, R. C. & Collins, A. G. Ten simple rules for the computational modeling of behavioral data. *eLife* **8**, e49547 (2019).
74. Akaishi, R., Umeda, K., Nagase, A. & Sakai, K. Autonomous mechanism of internal choice estimate underlies decision inertia. *Neuron* **81**, 195–206 (2014).
75. Akaike, H. A new look at the statistical model identification. *IEEE Trans. Autom. Control* **19**, 716–723 (1974).
76. Pnevmatikakis, E. A. & Giovannucci, A. NoRMCorre: an online algorithm for piecewise rigid motion correction of calcium imaging data. *J. Neurosci. Methods* **291**, 83–94 (2017).
77. Zhou, P. et al. Efficient and accurate extraction of in vivo calcium signals from microendoscopic video data. *eLife* **7**, e28728 (2018).
78. Giovannucci, A. et al. CaImAn an open source tool for scalable calcium imaging data analysis. *eLife* **8**, e38173 (2019).
79. Johnston, K. G. et al. Tracking longitudinal population dynamics of single neuronal calcium signal using SCOUT. *Cell Rep. Methods* **2**, 100207 (2022).
80. O'Neill, P.-K. et al. The representational geometry of emotional states in basolateral amygdala. *Nat. Neurosci.* **29**, 1654–1666 (2026).
81. Oord, A. van den, Li, Y. & Vinyals, O. Representation learning with contrastive predictive coding. Preprint at https://doi.org/10.48550/arXiv.1807.03748 (2019).
82. Lazic, S. E. The problem of pseudoreplication in neuroscientific studies: is it affecting your analysis?. *BMC Neurosci* **11**, 5 (2010).
83. Bussell, J. J. et al. Representations of the intrinsic value of information in mouse orbitofrontal cortex. *Zenodo* https://doi.org/10.5281/zenodo.20450673 (2026).
84. Bussell, J. J. et al. Representations of the intrinsic value of information in mouse orbitofrontal cortex. *Zenodo* https://doi.org/10.5281/zenodo.20452041 (2026).
85. Bussell, J. J. et al. Representations of the intrinsic value of information in mouse orbitofrontal cortex. *Zenodo* https://doi.org/10.5281/zenodo.20466860 (2026).
86. Bussell, J. J. et al. Representations of the intrinsic value of information in mouse orbitofrontal cortex. *Zenodo* https://doi.org/10.5281/zenodo.20470580 (2026).
87. Bussell, J. J. et al. Representations of the intrinsic value of information in mouse orbitofrontal cortex. *Zenodo* https://doi.org/10.5281/zenodo.20470622 (2026).
88. Bussell, J. J. et al. Representations of the intrinsic value of information in mouse orbitofrontal cortex. *Zenodo* https://doi.org/10.5281/zenodo.20477351 (2026).
89. Bussell, J. J. et al. Representations of the intrinsic value of information in mouse orbitofrontal cortex. *Zenodo* https://doi.org/10.5281/zenodo.20479276 (2026).
90. Bussell, J. J. et al. Representations of the intrinsic value of information in mouse orbitofrontal cortex. *Zenodo* https://doi.org/10.5281/zenodo.20480778 (2026).
91. Bussell, J. J. et al. Imaging data for Representations of the intrinsic value of information in mouse orbitofrontal cortex. *Figshare* https://doi.org/10.25452/figshare.plus.32582997 (2026).

Acknowledgements

We thank members of the Axel lab, E. Schaffer, L. Posani and M. Mathis for helpful discussions. We would also like to thank the research assistants T. Hannah, R. Singh, A. Viswanathan, D. Bingul, A. Awak and M. Sharma Campbell who performed mouse behavioral training as well as N. Zabello and the staff of the Zuckerman Institute for Comparative Medicine for their expert animal care. We would like to acknowledge T. Tabachnik and the Zuckerman Institute Advanced Instrumentation Core for their help with design of behavioral chambers. We would like to acknowledge the team from Stellate Communications for their help with mouse illustration. We would also like to acknowledge A. Nemes, M. D'Arduini, C. Eccard and M. Gutierrez for their laboratory support and assistance in drafting this manuscript.

Author contributions

Study conceptualization by R.A., J.J.B., E.S.B.-M. and K.R. Methodology by J.J.B., R.P.B., D.M., E.S.B.-M., K.R., L.F.A. and R.A. Formal analysis by J.J.B., R.P.B., D.M. and L.F.A. Investigation by J.J.B. Visualization by J.J.B. Software by J.J.B., R.P.B. and D.M. Funding acquisition by R.A., L.F.A. and K.R. Supervision by R.A. and K.R. Writing—original draft by J.J.B. and R.A. Writing—review and editing by J.J.B., R.A., L.F.A., E.S.B.-M. and R.P.B.

Funding

This work was supported by the Simons Foundation (to J.J.B., L.F.A., R.P.B., D.M. and K.R.); the Howard Hughes Medical Institute (to R.A.); NIH grant nos. MH106435, R01MH110594 and R01MH116937 (supporting E.S.B.-M.) and RF1 DA056403 (to R.P.B., D.M. and K.R.); an NSF CAREER Award (no. 2427124 to K.R.); the James S. McDonnell Foundation (no. 220020466 to K.R.); the McKnight Endowment Fund (to K.R.); the Gatsby Charitable Foundation (to L.F.A.); and the CIFAR Azrieli Global Scholar Program (to R.P.B., D.M. and K.R.). This work has been made possible in part by a gift from the Chan Zuckerberg Initiative Foundation to establish the Kempner Institute for the Study of Natural and Artificial Intelligence at Harvard University. The funders had no role in study design, data collection and analysis, decision to publish, or preparation of the manuscript.

Competing interests

The authors declare no competing interests.

Additional information

Extended data is available for this paper at https://doi.org/10.1038/s41593-026-02377-y.

Supplementary information The online version contains supplementary material available at https://doi.org/10.1038/s41593-026-02377-y.

Correspondence and requests for materials should be addressed to Jennifer J. Bussell or Richard Axel.

Peer review information *Nature Neuroscience* thanks Paul Masset and the other, anonymous, reviewer(s) for their contribution to the peer review of this work.

https://doi.org/10.1038/s41593-026-02377-y

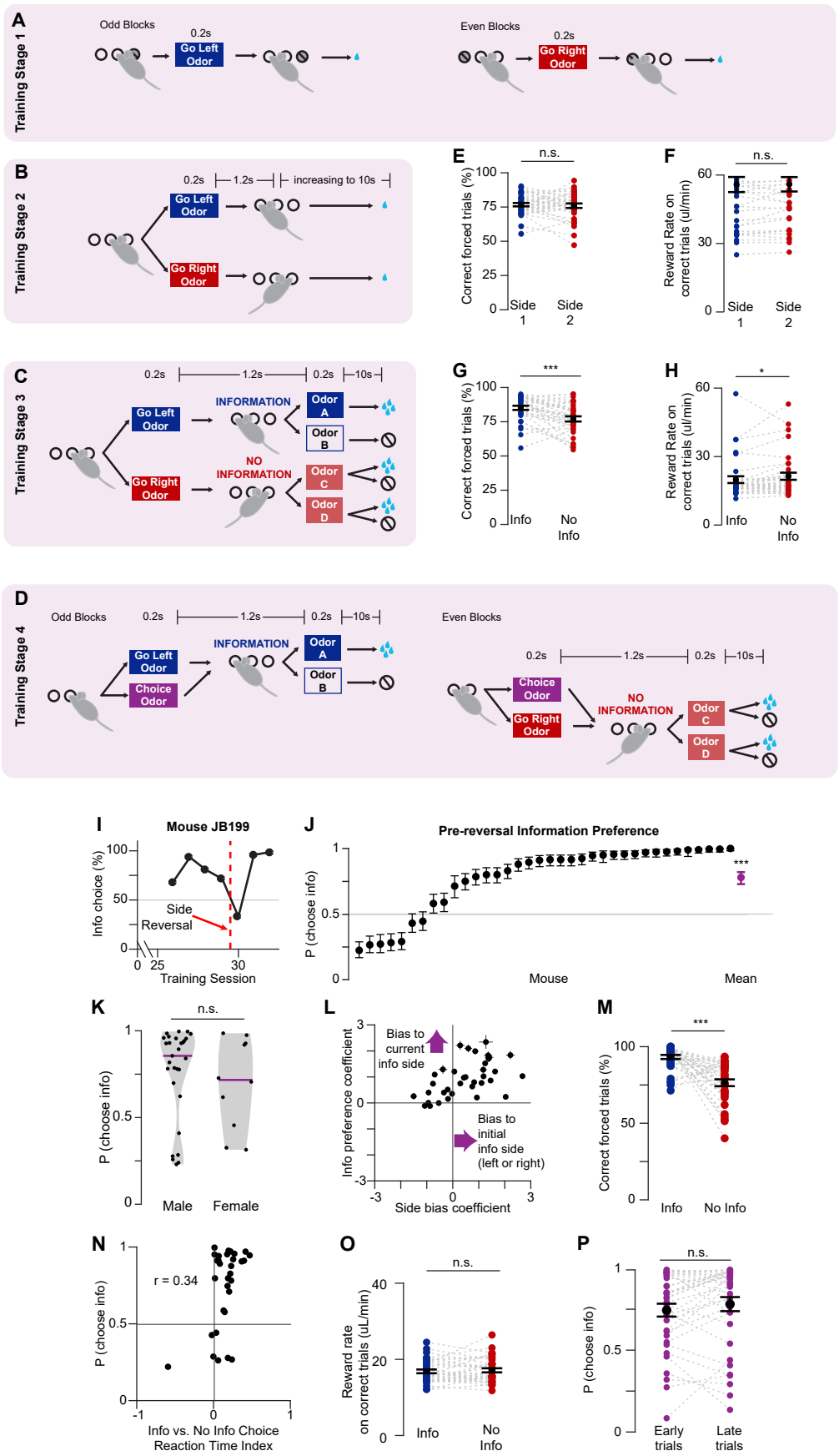

Extended Data Fig. 1 | See next page for caption.

https://doi.org/10.1038/s41593-026-02377-y

Extended Data Fig. 1 | Task training and behavioral analysis. (**A**) Initial task training stage with alternating blocks with one side port covered. Mice learn to first receive odor in the center port and then enter the uncovered side port. (**B**) Second task training stage in which mice learn that odor directs them to either the left or right side on pseudo-alternating trials and the delay to reward is gradually increased. (**C**) Third task training stage in which rewards are made probabilistic and side port odors (information and no information) are introduced. (**D**) Fourth task training stage in which the free choice center port odor is introduced in alternating blocks of trials on the information or no information side such that mice learn they can choose either side on free choice trials. (**E**) Correct performance of forced trials in training stage 2, points for single animals, black shows mean and std err across animals, two-sided Wilcoxon sign rank test, p = 0.66, N = 36 mice. (**F**) Reward rate on forced side 1 (future information) versus side 2 (future no information) trials in training stage 2, plot as in (E), two-sided Wilcoxon sign rank test, p = 0.41, N = 36 mice. (**G**) Correct performance of forced trials in training stage 3, plot as in (E), two-sided Wilcoxon sign rank test, $p = 1.35x10^{-4}$, N = 36 mice. (**H**) Reward rate on forced information versus forced no information side trials in training stage 3, plot as in (E), two-sided Wilcoxon sign rank test, p = 0.013, N = 36 mice. (**I**) Information preference for an example mouse. Dotted line shows the reversal of the information side port. (**J**) Initial information preference prior to side reversal. Gray bars show mean and 95% confidence interval for each mouse, trial sample sizes listed in Supplementary Table 1. Purple point shows mean and std err across animals, two-sided Wilcoxon sign rank test, $p = 5.20x10^{-6}$, N = 36 mice. (**K**) Information preference for male and female mice. Points for single animals, purple line shows mean, two-sided Wilcoxon sign-rank test, p = 0.52, N = 36 mice. (**L**) Logistic regression coefficient for side and information choice in each animal across all choices on both sides. Points represent single animals with lines for 95% confidence interval. (**M**) Correct performance of forced trials. Plot as in (E), two-sided Wilcoxon sign rank test, $p = 1.93x10^{-5}$, N = 36 mice. (**N**) Per-animal choice trial reaction time index (mean reaction time no info-mean reaction time info)/(mean reaction time info + mean reaction time no info)) versus mean information preference prior to side reversal. Two-sided Spearman's correlation, p = 0.031, N = 36 mice. (**O**) Reward rate on correct forced information versus forced no information trials, two-sided Wilcoxon sign rank test, p = 0.16, N = 36 mice. (**P**) Information preference on trials in first vs. last third of session. Plot as in (**E**), Wilcoxon sign-rank test, p = 0.85, N = 36 mice.

https://doi.org/10.1038/s41593-026-02377-y

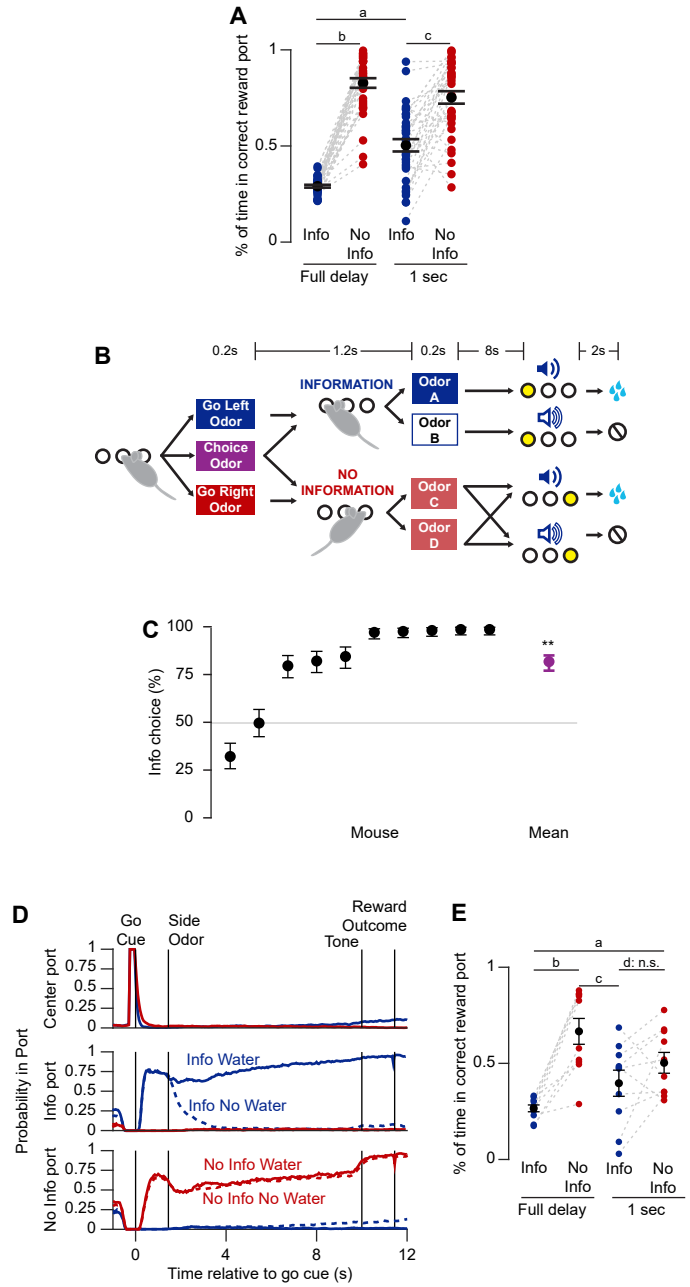

Extended Data Fig. 2 | Mice leave both ports in a task variant with early reward signal on all trials. (**A**) Probability of nose poking in the correctly chosen side port on forced information versus no information trials, across the full delay from the end of side port odor delivery to reward outcome and in the first second following side port odor delivery in the main task, points show the mean for each mouse, black shows mean +/- std err across animals, Friedman's ANOVA with Tukey-Cramer correction for multiple comparisons, a: $p = 0.0076$, b: $p = 3.53 \times 10^{-15}$, c: $p = 0.0029$, N = 36 mice. (**B**) Task variant with cue for outcome delivery on all trials. The correct reward port was illuminated and a tone indicated whether the trial was rewarded or unrewarded 2 s prior to possible water delivery on all trials. (**C**) Information preference in the cued outcome task variant in (B). Gray bars show mean and 95% confidence interval for each mouse, N = 200 trials per mouse. Purple bar shows mean and std err across animals, two-sided Wilcoxon sign rank test, **$p = 0.010$, N = 10 mice. (**D**) Probability of nose poking in each port by trial type in the cued outcome task variant, N = 10 mice. (**E**) Probability of nose poking in as in (A) but for the cued outcome task variant, Friedman's ANOVA with Tukey-Cramer correction for multiple comparisons, a: $p = 0.017$, b: $p = 3.95 \times 10^{-4}$, c: $p = 0.046$, d: $p = 0.40$, N = 10 mice.

https://doi.org/10.1038/s41593-026-02377-y

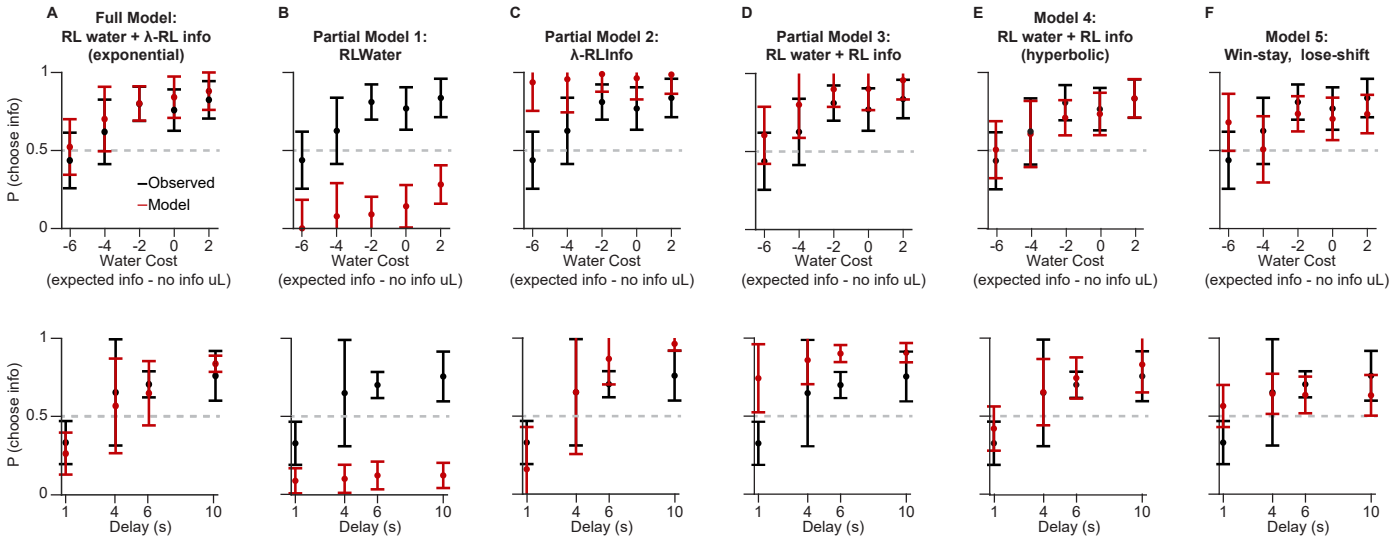

Extended Data Fig. 3 | An ablation study of our decision model in Fig. 1 and Methods was performed to show the behavioral effects of dropping each of the key model terms and variables, N = 10 mice total including 4 fit only for water cost experiments. (**A**) Full model with Rescorla-Wagner water term and exponential delay-discounted information term from Fig. 1. (**B**) When the information value Rescorla-Wagner term was dropped (RLwater), the ability to predict information preference completely collapsed. The predicted preference dropped below 50% because the model was fit to actual mouse choices and trial variables, and the mice on average preferred information. (**C**) When the Rescorla-Wagner term of water value was dropped but the exponential delay-discounted Information term was kept (λ-RLinfo), the model overestimated the information preference at the highest delay value and underestimated the Information preference at the smallest delay value. It also completely failed to predict the behavior in the water value-tuning experiments. (**D**) When the discount exponent was dropped on the information value term, so that the information value was unchanged at all delay durations (RLwater + RLinfo), the model failed to predict the results of the delay tuning experiment. (**E**) A hyperbolic variant of the full model was tested, finding $\kappa = 0.512 +/- 302$. This model qualitatively captured the major delay and water tuning trends, and performed comparably though with slightly worse AIC and accuracy than the exponential λ model. (**F**) Last, we tested a probabilistic win-stay, lose-shift model where mice have sigmoid transformed regression coefficients for each possible previous trial type and outcome (info rewarded, no-info rewarded, info unrewarded, no-info unrewarded), as well as a flat information preference across conditions that is an additional fit parameter. For example, in potential WSLS behavior mice may want to switch more often after unrewarded trials. This model predicted overall average behavior in a coarse-grained way, but failed to predict behavioral changes as relative water value and delay duration were tuned especially at the ends of the tuning spectrums. Error bars are 95% CI.

https://doi.org/10.1038/s41593-026-02377-y

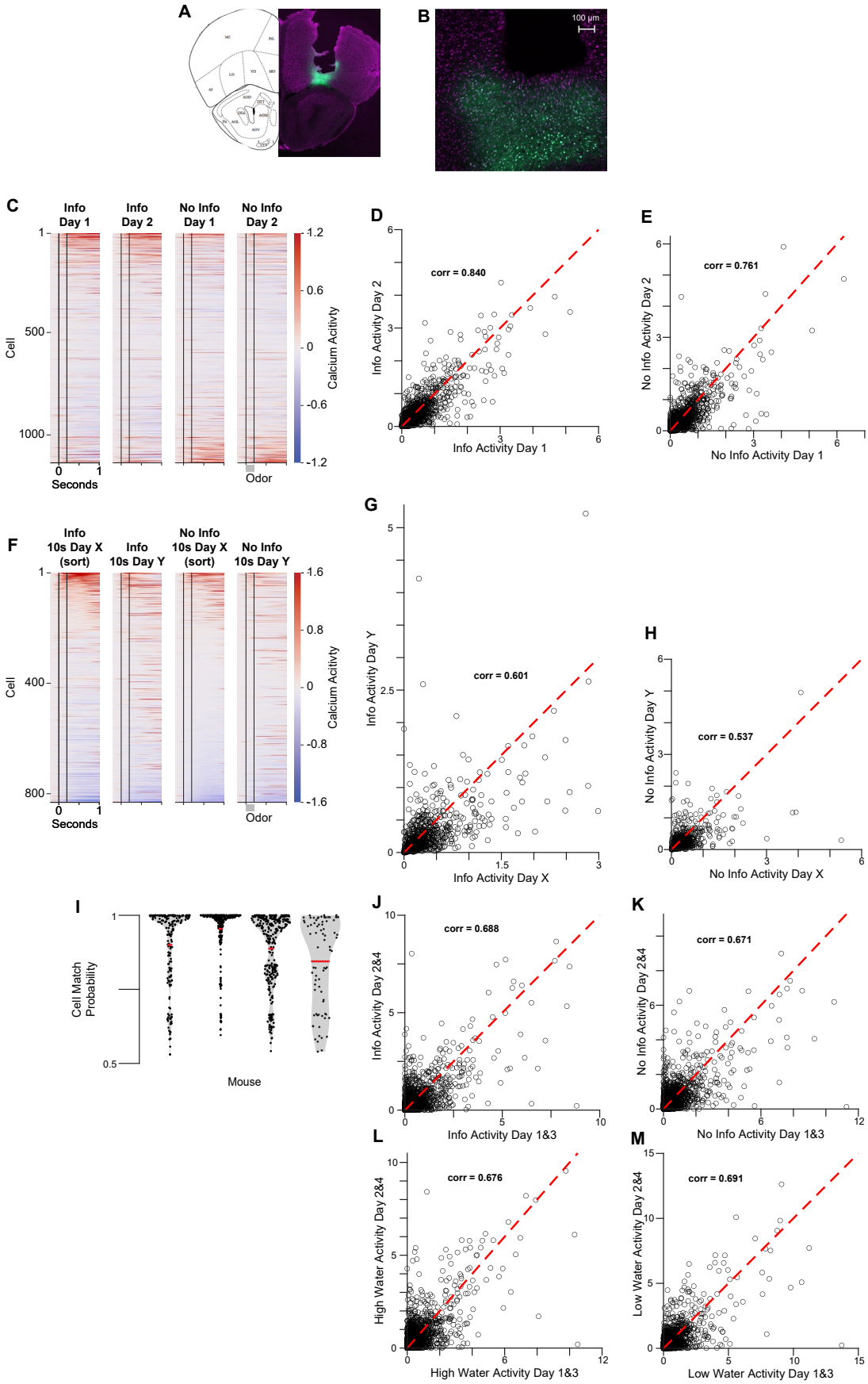

Extended Data Fig. 4 | See next page for caption.

https://doi.org/10.1038/s41593-026-02377-y

Extended Data Fig. 4 | Activity of registered OFC cells is stable across sessions. (**A**) Representative image of GCaMP-expressing virus (green) and GRIN lens location, with neuronal cell bodies in magenta. Coronal section of an example brain and aligned atlas view, 2.46 mm from Bregma. (**B**) Magnified view of A. (**C**) Population responses to center port odors on forced information and forced no information on consecutive days 1 and 2 with information on the same side. Cells in all columns sorted by info day 1. (**D,E**) Responses to center port odors are highly correlated across consecutive days. Plot shows correlation of mean calcium activity in a 1 s interval after the center port odor on information forced (**D**) and no information forced (**E**) trials on day 1 versus day 2 across cells. Two-sided Pearson correlation, $p < 10^{-308}$ (computer precision) (**D**) and $p < 10^{-308}$ (computer precision) (**E**), N = 2276 cell-day pairs (a point for each cell for each day). (**F**) Activity across days surrounding task delay changes. Population responses to center port odors on forced information and forced no information on 'Day X,' the last 2 days of testing with a 10 s delay, and 'Day Y,' the last two days of testing after returning to a 10 s delay, with the two days separated by an intervening block of testing at a 1 s delay. Days X and Y mean 29 days apart. (**G,H**) Responses to center port odors in the same task configuration are highly correlated despite intervening weeks of training on different task parameters. Plot shows correlation of mean calcium activity in a 1 s interval after the center port odor on information (**G**) and no information (**H**) trials on Day X versus Day Y across cells. Two-sided Pearson correlation, (**G**) $p = 2.28x10^{-82}$, (**H**) $p = 4.44x10^{-63}$, N = 827 cells with activity pooled from two days before learning versus two days after learning. (**I**) Probabilities of correct match for each matched cell pair by mouse in SCOUT cell registration of the 4 sessions analyzed in 4 center port odor task (Fig. 4). Red line indicates mean probability. N = 195, 297, 317, and 78 cells. (**J-M**) Responses to center port odors on consecutive days in the 4 center odor task are highly correlated. Correlation of mean calcium activity in a 1 s interval after the center port odor on information (**J**) and no information (**K**) trials on days 1 and 3 (first days pre- and post-side reversal) versus days 2 and 4 (second days pre- and post-side reversal) across cells. Correlation of mean calcium activity in a 1 s interval after the center port odor on high (**L**) and low (**M**) trials on days 1 and 3 (first days pre- and post-side reversal) versus days 2 and 4 (second days pre- and post-side reversal) across cells. Two-sided Pearson correlation, $p = 7.66x10^{-271}$ (**J**), $p = 3.25x10^{-252}$ (**K**), $p = 4.58x10^{-258}$ (**L**), $p = 1.07x10^{-273}$ (**M**), N = 1928 cell-day pairs (a point for each cell for each set of days).

https://doi.org/10.1038/s41593-026-02377-y

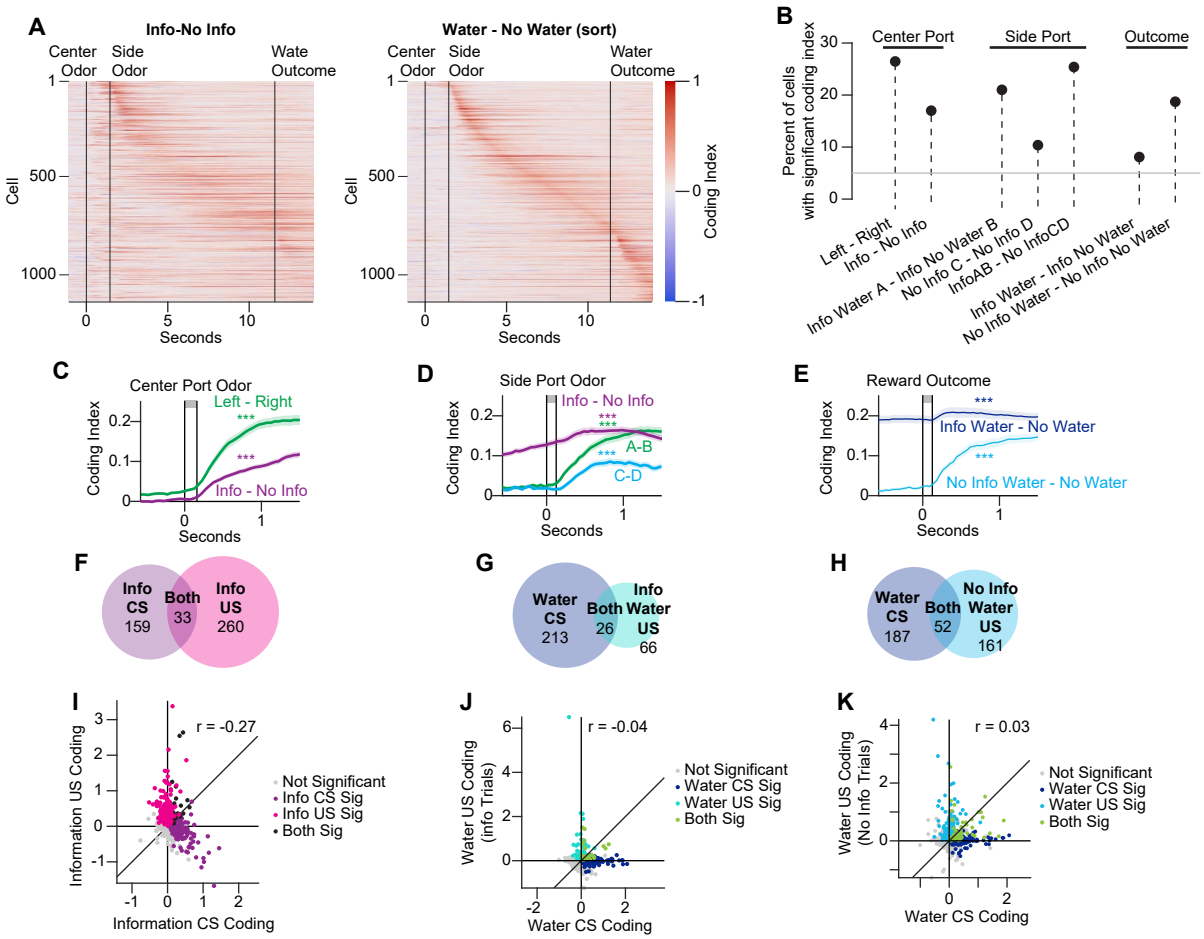

Extended Data Fig. 5 | OFC represents both information and water as conditioned and unconditioned stimuli. (**A**) Left, information coding index across the population. Right, water coding index. Cells sorted in both by water coding index. (**B**) Percent of cells encoding each differential response, with observed coding index difference between the two conditions greater than 95% of 1000 permutations of trials between the two conditions, N = 1138 cells. (**C-E**) Population mean coding indices. Shaded area shows standard error. (**C**) Coding at center port odor, (**D**) at side port odor, (**E**) at reward outcome. Odor C-D activity difference reflects that odor D is provided on 75%, whereas odor C is provided on 75%, of no information trials., ***p < 0.001, permutation test. (**F-H**) Overlap between cells comprising value representations, chi-square test, N = 1138 cells. (**F**) Info CS versus info US, p = -0.095. (**G**) Water CS versus water US on information trials, p = 0.075. (**H**) Water CS versus water US on no information, p = 0.18. (**I-K**) Relationship between CS and US coding (coding index 1 s after – 1 s before relevant event) for (**I**) information, p = 1.00 (**J**) water on information trials, p = 0.90, (**K**) water on no information trials, p = 0.19, two-sided Pearson's correlations shown.

https://doi.org/10.1038/s41593-026-02377-y

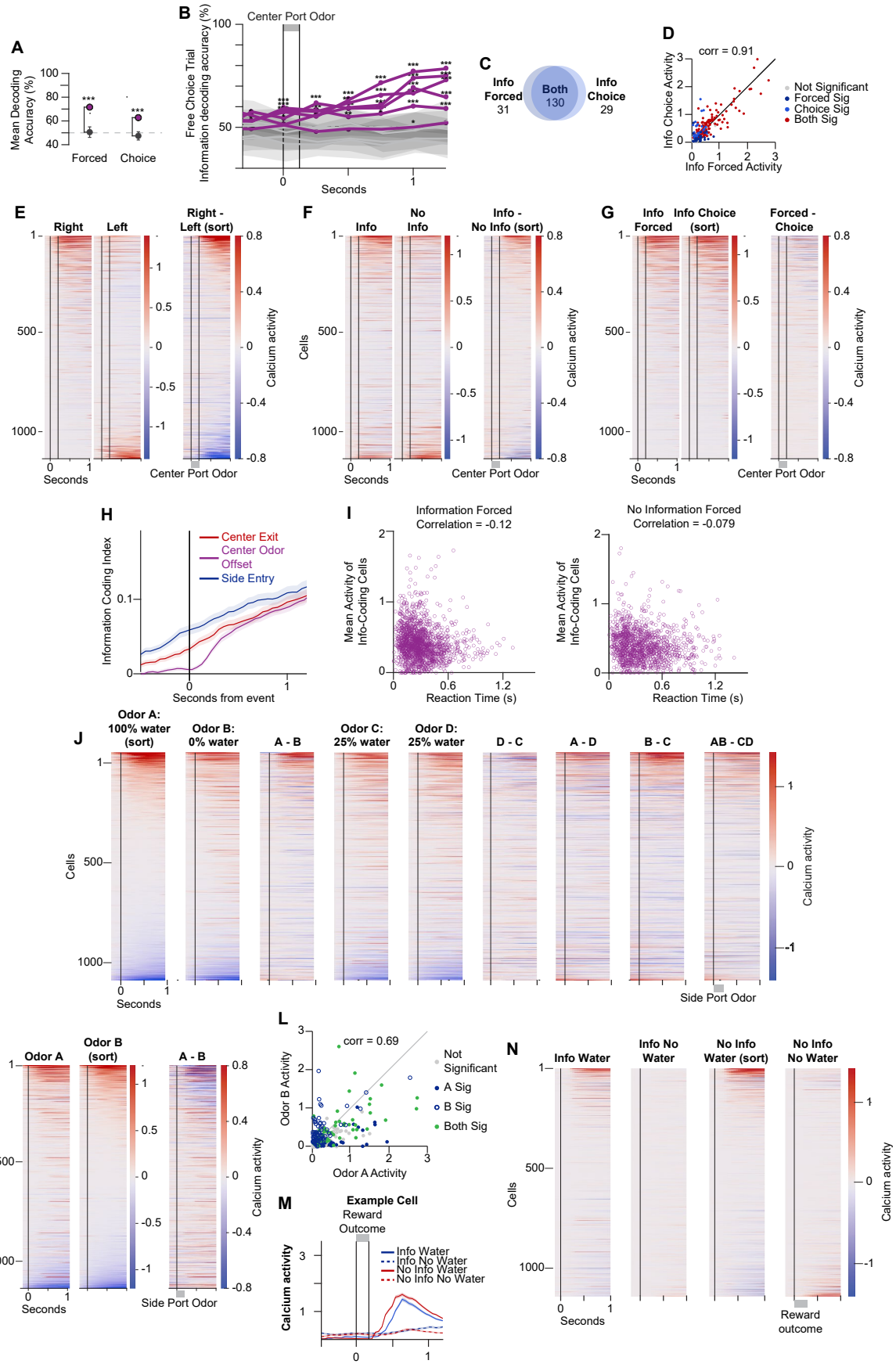

Extended Data Fig. 6 | See next page for caption.

https://doi.org/10.1038/s41593-026-02377-y

Extended Data Fig. 6 | OFC cells respond to center and side port odors and the receipt of water. (**A**) Mean information decoding accuracy at center port odor on forced and choice trials for pseudo-population data across mice. *** forced trials $8.6x10^{-22}$, choice trials $4.9x10^{-19}$ versus null model, one-sided z-score, N = 10 cross-validations. (**B**) Information versus no information decoding accuracy on choice trials. Purple, individual animals, grey, shuffled null distributions. ***$p < 0.001$, **$p < 0.01$, *$p < 0.05$, one-sided z-score. Exact p values listed in Supplementary Table 2, N = 10 cross-validations. (**C**) Overlap between cells responding to center port odor on forced and free choice information trials, $p = 2.65x10^{-153}$, chi-square test, N = 1138 cells. (**D**) Correlation between center port odor responses (1 s after odor − 1 s before odor) on forced and choice information trials. Two-sided Pearson's correlation, $p < 10^{-308}$ (computer precision), N = 1138 cells. (**E**) Population responses to center port odors directing to the right or left side port. Each cell's mean activity on left and right forced trials, and the difference between them, shown. Cells sorted by difference. (**F**) Population responses to center port odors directing to information or no information on forced trials. Plots as in (**E**). (**G**) Population responses to center port odors on forced and choice information trials and their difference. Cells sorted by information choice trial activity. Plots as in (**E**). (**H**) Population information coding activity aligned to choice-related events. Lines show mean information coding index; shading shows standard error. (**I**) Correlation between information-predicting activity and reaction time on, left, forced information and, right, forced no information trials. Each point shows reaction time versus mean activity across information CS-encoding cells in 1 s interval after center odor on a single trial. Two-sided Pearson's correlation, left $p = 2.78x10^{-5}$, N = 1606 information forced trials, right p = 0.011, N = 1310 no information forced trials. (**J**) Population responses to side port odors. Columns sorted by odor A activity. (**K**) Population responses to side port odors A and B, sorted by response to odor B. (**L**) Correlation between responses to odor A and odor B (1 s after odor − 1 s before odor). Two-sided Pearson's correlation, $p = 2.40x10^{-159}$, N = 1138 cells. (**M**) Activity of an example water US-encoding cell at reward outcome. Line shows mean, shading shoes standard error. (**N**) Population responses to reward outcome, columns sorted by response to water reward on no information trials.

https://doi.org/10.1038/s41593-026-02377-y

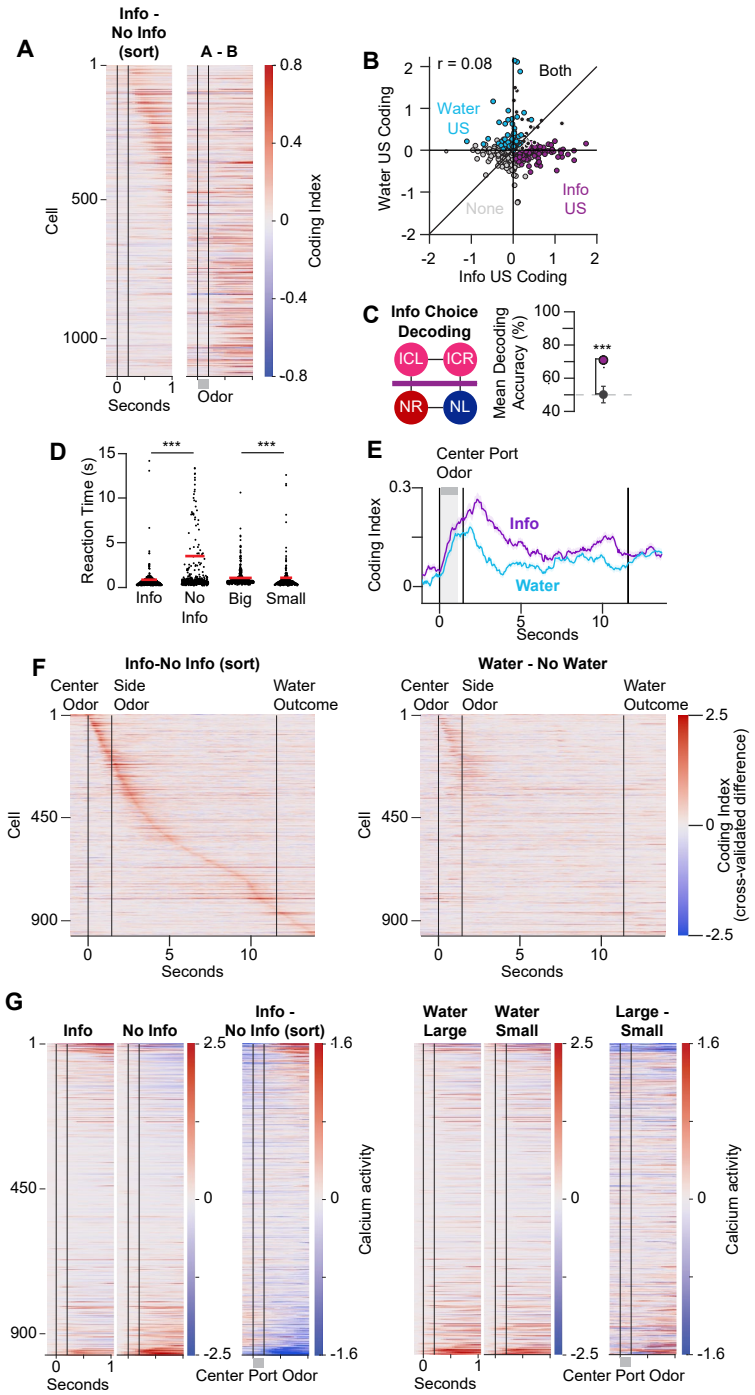

Extended Data Fig. 7 | Information and water value representations are distinct. (**A**) Information CS and water CS coding across OFC cells in the main task. Left, information coding index at the center port odor across the population. Right, water coding index at the Information side port odor. Both sorted by information coding index. (**B**) Relationship between information US coding (coding index 1 s after −1 s before odor presentation) and water US coding (coding index 1 s after −1 s before water reward), two-sided Pearson correlation, p = 0.0044, N = 1138 cells. (**C**) Decoding schematic and mean decoding accuracy at center port odor on choice information versus forced no information trials for pseudo-population data across mice. P = 9.6x10-36 versus null model, one-tailed z-score, N = 10 cross-validations. (**D**) Reaction times by trial type prior to side reversal for the four center odor task. Purple indicates mean, two-sided Wilcoxon rank sum test, info-no info p = 3.80×10^{-25}, N = 1105 trials, big vs small water amount p = 5.38×10^{-24}, N = 941 trials. (**E**) Population mean information and water coding indices in the four center odor task. Shading shows standard error. Gray vertical shading shows 1 s post-center port odor CS coding analysis window. (**F**) Mean information (left) and water (right) coding indices across the population in the four center odor task. Cells in both plots sorted by information coding index. (**G**) Population responses to center port odors in the four center odor task. Cells sorted by the information-no information difference.

https://doi.org/10.1038/s41593-026-02377-y

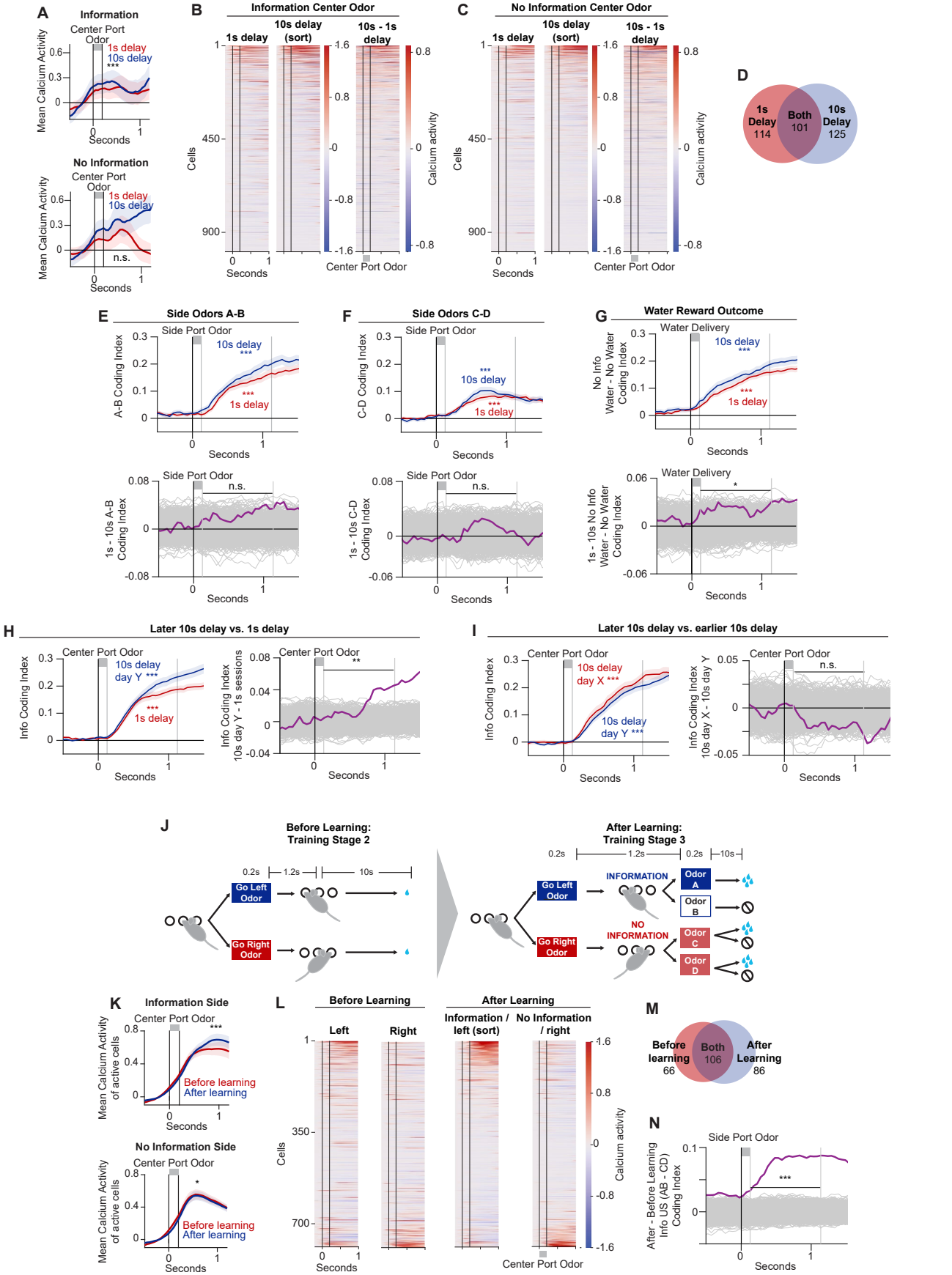

Extended Data Fig. 8 | See next page for caption.

https://doi.org/10.1038/s41593-026-02377-y

Extended Data Fig. 8 | The OFC representation of predicted information scales with value and emerges with learning. (**A**) Mean population calcium activity at the center port on forced information (top) and forced no information (bottom) trials, in sessions with a 1 s and 10 s delay. Shading shows standard error, info $p = 2.78x10^{-11}$, no info p = 0.093, two-sided sign rank test, trial sample sizes in Supplementary Table 5. (**B**) Population activity on forced information trials in 1 s and 10 s delay sessions. Cells sorted by 10 s delay activity. (**C**) As in (B), but for forced no information trials. (**D**) Overlap between information CS cells in 1 s and 10 s delay sessions, $p = 1.09x10^{-21}$, chi-square test, N = 993 cells. (**E**, **F**, **G**) Top, population mean coding index in sessions with 1 s versus 10 s delay. Mean and standard error shown. ***p < 0.001, permutation test. Bottom, difference between coding index in 10 s – 1 s delay sessions (purple). Gray shows shuffled data, permutation test, trial sample sizes in Supplementary Table 5. (**E**) Water coding index at the information side port, p = 0.13, (**F**) Coding index for odor C – odor D at the side port, p = 0.37, (**G**) Water coding index on no information trials at water delivery, p = 0.042. (**H**) We compared 1 s delay sessions with a second separate set of later sessions with the delay returned to 10 s. Left, population mean information coding index at the center port in sessions with 10 s versus 1 s delay. 10 s delay sessions recorded following 1 s delay sessions. Mean and standard error shown. ***p < 0.001, permutation test. Right, difference between information coding index at the center port in 1 s – later 10 s delay sessions (purple). Gray shows shuffled data, **p = 0.0020, permutation test, trial sample sizes in Supplementary Table 6. (**I**) We compared two sets of 10 s delay sessions, one earlier before the 1 s sessions, Day X, and one later after decreasing the delay to 1 s and then returning it to 10 s, Day Y. Left, population mean information coding index at the center port in Day X 10 s delay sessions and Day Y 10 s delay sessions, ***p < 0.001, permutation test. Right, difference between information coding index at the center port in 10 s Day X –10 s Day Y delay sessions (purple). Gray shows shuffled data, p = 0.93, permutation test, trial sample sizes in Supplementary Table 7. (**J**) Schematic of learning across training stages when information is introduced by providing odor at the side port and making water rewards probabilistic. (**K**) Mean population calcium activity across odor-responding cells at the center port on information side (top) and no information side (bottom) trials, in sessions before and after learning. Shading shows standard error, information side (top), $***p = 1.45x10^{-6}$, two-sided sign rank test, N = 173906 information trials before learning, 177814 information trials after learning. No information side (bottom), p = 0.03, two-sided sign rank test, 167067 no information trials before learning, 141665 no information trials after learning. (**L**) Population activity at the center port across learning. Left, activity on forced 'left' (port 1) and forced 'right' (port 2) trials. Right, activity on forced information (port 1) and forced no information (port 2) trials. Cells sorted by activity on forced information trials after learning. Left/right ports counterbalanced across animals. (**M**) Overlap between left-right CS (before learning) and information CS (after learning) cells, $p = 9.11\times10^{-29}$, chi-square test, N = 788 cells. (**N**) Emergence of information US coding. Difference between information coding index at the side port in sessions before and after learning (purple). Gray shows shuffled data, ***p < 0.001, permutation test, trial sample sizes in Supplementary Table 4.

https://doi.org/10.1038/s41593-026-02377-y

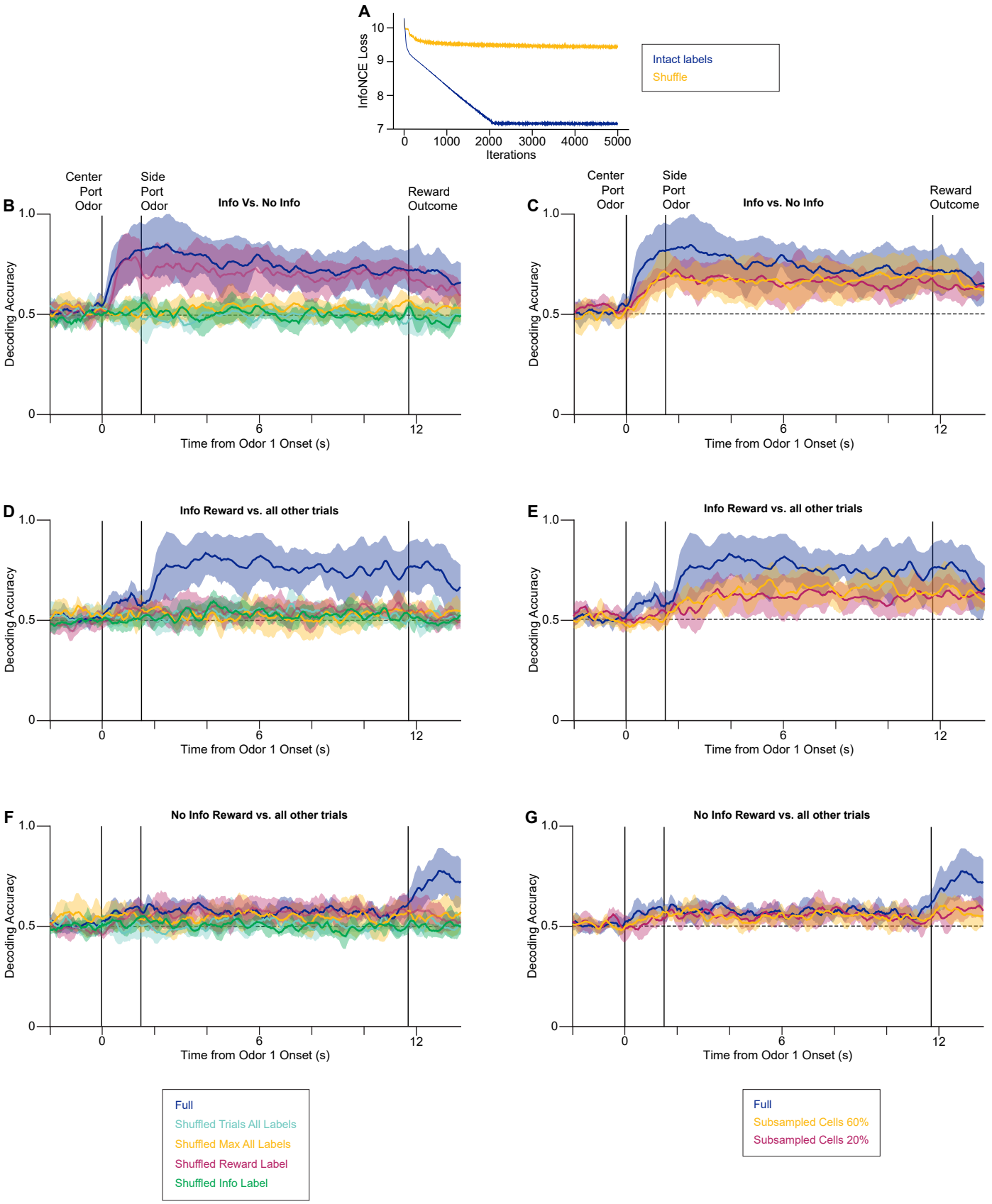

Extended Data Fig. 9 | See next page for caption.

https://doi.org/10.1038/s41593-026-02377-y

Extended Data Fig. 9 | Shuffling data labels controls for CEBRA embedding model fit. (**A**) Comparison of the model's contrastive loss as measured by InfoNCE (Info Noise-Contrastive Estimation) with intact versus shuffled labels. Lower loss suggests a better fit model. Decoding accuracy of (**B**) information trial type versus no information trial type for all trials, (**D**) presence of reward on information trials and (**F**) presence of reward on no information trials. In (**b**, **d**, and **f**), the legends are defined as follows. In the 'shuffled trials all labels' condition, the assignment of trials was randomized relative to their original time-varying labels, for all the label types, but we left the matching between labels and the time they were assigned in a trial intact. In the 'shuffled max all labels' condition, we randomly scrambled both the trial- and the time affiliation of a given label, for all label types, thus resulting in the maximum amount of signal scrambling. For the 'shuffled info label' condition, we only scrambled the trial-label assignment for the 'info vs no info' label type, leaving all others intact. For the 'shuffled reward label' condition, we only scrambled the trial-label assignment for the 'rewarded vs unrewarded' label, leaving all others intact. 'Full' is the finalized intact labels for the full model. Results are reported as an average across 5 runs, using different random seeds to achieve the train/test allocation. (**C**, **E**, **G**) Models fit to only random sub-populations of cells were also used as controls to show that embedding quality deteriorated with reduced sample size. 20% (magenta) and 60% (orange) of OFC neurons recorded were sub-sampled and compared to the full sample (blue). Each sampling was the average of five runs, using five different random seeds to subsample the cells. Results are reported averaged across sessions, animals and runs with error bars to show 95% confidence interval.

nature portfolio

Corresponding author(s): Richard Axel

Last updated by author(s): Dec 8, 2025

Reporting Summary

Nature Portfolio wishes to improve the reproducibility of the work that we publish. This form provides structure for consistency and transparency in reporting. For further information on Nature Portfolio policies, see our Editorial Policies and the Editorial Policy Checklist.

Statistics

For all statistical analyses, confirm that the following items are present in the figure legend, table legend, main text, or Methods section.

n/a	Confirmed	
☐	☒	The exact sample size (*n*) for each experimental group/condition, given as a discrete number and unit of measurement
☐	☒	A statement on whether measurements were taken from distinct samples or whether the same sample was measured repeatedly
☐	☒	The statistical test(s) used AND whether they are one- or two-sided *Only common tests should be described solely by name; describe more complex techniques in the Methods section.*
☒	☐	A description of all covariates tested
☐	☒	A description of any assumptions or corrections, such as tests of normality and adjustment for multiple comparisons
☐	☒	A full description of the statistical parameters including central tendency (e.g. means) or other basic estimates (e.g. regression coefficient) AND variation (e.g. standard deviation) or associated estimates of uncertainty (e.g. confidence intervals)
☐	☒	For null hypothesis testing, the test statistic (e.g. *F*, *t*, *r*) with confidence intervals, effect sizes, degrees of freedom and *P* value noted *Give P values as exact values whenever suitable.*
☒	☐	For Bayesian analysis, information on the choice of priors and Markov chain Monte Carlo settings
☒	☐	For hierarchical and complex designs, identification of the appropriate level for tests and full reporting of outcomes
☐	☒	Estimates of effect sizes (e.g. Cohen's *d*, Pearson's *r*), indicating how they were calculated

Our web collection on statistics for biologists contains articles on many of the points above.

Software and code

Policy information about availability of computer code

Data collection	Behavioral data were collected with Matlab v2016b-2021a using Bpod open-source code from Sanworks (https://github.com/sanworks/Bpod_Gen2) and custom protocols. Neural data were collected with Inscopix Data Acquisition Software v2.3.0 and pre-processed using Python code from Inscopix Data Processing Software v1.9.5 Python API.
Data analysis	Behavior and calcium activity data were analyzed using custom code in Matlab v2021a. Imaging recordings were processed using open-source algorithms NormCorre (https://github.com/flatironinstitute/NoRMCorre) and CNMF-E (https://github.com/zhoupc/CNMF_E). Latent variable neural data models were created using CEBRA (https://cebra.ai/) Decoding analyses were performed using Decodanda (https://github.com/lposani/decodanda). Code used to generate and analyze the data and create the figures is available at https://github.com/jjbussell/Bussell2026InfoValue.

For manuscripts utilizing custom algorithms or software that are central to the research but not yet described in published literature, software must be made available to editors and reviewers. We strongly encourage code deposition in a community repository (e.g. GitHub). See the Nature Portfolio guidelines for submitting code & software for further information.

Data

Policy information about availability of data

All manuscripts must include a data availability statement. This statement should provide the following information, where applicable:

- Accession codes, unique identifiers, or web links for publicly available datasets
- A description of any restrictions on data availability
- For clinical datasets or third party data, please ensure that the statement adheres to our policy

The behavioral and neural data generated and analyzed in this study are available in Zenodo with the following identifiers: https://doi.org/10.5281/zenodo.2045067383 (behavior), https://doi.org/10.5281/zenodo.2045204184 (main imaging data), https://doi.org/10.5281/zenodo.2046686085 (imaging data-learning), https://doi.org/10.5281/zenodo.2047058086 (imaging data-delay sessions), https://doi.org/10.5281/zenodo.2047062287 (task with 4 center port odors, information vs. water value), https://doi.org/10.5281/zenodo.2047735188 (imaging pipeline files JB413, JB424, JB425, JB426), https://doi.org/10.5281/zenodo.2047927689 (imaging files JB432, JB433, JB434, JB483, JB484), https://doi.org/10.5281/zenodo.2048077890 (imaging files JB506, JB507, JB509). Pre-processed and motion corrected calcium imaging video files are available in Figshare with the identifier https://doi.org/ 10.25452/figshare.plus.3258299791. Due to their large size, the raw calcium imaging video files are available from the corresponding author upon reasonable request.

Research involving human participants, their data, or biological material

Policy information about studies with human participants or human data. See also policy information about sex, gender (identity/presentation), and sexual orientation and race, ethnicity and racism.

Reporting on sex and gender	*Use the terms sex (biological attribute) and gender (shaped by social and cultural circumstances) carefully in order to avoid confusing both terms. Indicate if findings apply to only one sex or gender; describe whether sex and gender were considered in study design; whether sex and/or gender was determined based on self-reporting or assigned and methods used.* *Provide in the source data disaggregated sex and gender data, where this information has been collected, and if consent has been obtained for sharing of individual-level data; provide overall numbers in this Reporting Summary. Please state if this information has not been collected.* *Report sex- and gender-based analyses where performed, justify reasons for lack of sex- and gender-based analysis.*
Reporting on race, ethnicity, or other socially relevant groupings	*Please specify the socially constructed or socially relevant categorization variable(s) used in your manuscript and explain why they were used. Please note that such variables should not be used as proxies for other socially constructed/relevant variables (for example, race or ethnicity should not be used as a proxy for socioeconomic status).* *Provide clear definitions of the relevant terms used, how they were provided (by the participants/respondents, the researchers, or third parties), and the method(s) used to classify people into the different categories (e.g. self-report, census or administrative data, social media data, etc.)* *Please provide details about how you controlled for confounding variables in your analyses.*
Population characteristics	*Describe the covariate-relevant population characteristics of the human research participants (e.g. age, genotypic information, past and current diagnosis and treatment categories). If you filled out the behavioural & social sciences study design questions and have nothing to add here, write "See above."*
Recruitment	*Describe how participants were recruited. Outline any potential self-selection bias or other biases that may be present and how these are likely to impact results.*
Ethics oversight	*Identify the organization(s) that approved the study protocol.*

Note that full information on the approval of the study protocol must also be provided in the manuscript.

Field-specific reporting

Please select the one below that is the best fit for your research. If you are not sure, read the appropriate sections before making your selection.

☒ Life sciences ☐ Behavioural & social sciences ☐ Ecological, evolutionary & environmental sciences

For a reference copy of the document with all sections, see nature.com/documents/nr-reporting-summary-flat.pdf

Life sciences study design

All studies must disclose on these points even when the disclosure is negative.

Sample size	Sample sizes were not predetermined, but our sample sizes are similar or larger than those in similar studies (Kuwabara et al. 2020).
Data exclusions	Mice that failed to learn the task (<15% of animals) were excluded from behavioral analysis.
Replication	Behavioral findings were reproduced across separately trained cohorts of animals.
Randomization	Information side and odors were pseudorandomly assigned across animals.

Blinding N/A

Behavioural & social sciences study design

All studies must disclose on these points even when the disclosure is negative.

Study description	*Briefly describe the study type including whether data are quantitative, qualitative, or mixed-methods (e.g. qualitative cross-sectional, quantitative experimental, mixed-methods case study).*
Research sample	*State the research sample (e.g. Harvard university undergraduates, villagers in rural India) and provide relevant demographic information (e.g. age, sex) and indicate whether the sample is representative. Provide a rationale for the study sample chosen. For studies involving existing datasets, please describe the dataset and source.*
Sampling strategy	*Describe the sampling procedure (e.g. random, snowball, stratified, convenience). Describe the statistical methods that were used to predetermine sample size OR if no sample-size calculation was performed, describe how sample sizes were chosen and provide a rationale for why these sample sizes are sufficient. For qualitative data, please indicate whether data saturation was considered, and what criteria were used to decide that no further sampling was needed.*
Data collection	*Provide details about the data collection procedure, including the instruments or devices used to record the data (e.g. pen and paper, computer, eye tracker, video or audio equipment) whether anyone was present besides the participant(s) and the researcher, and whether the researcher was blind to experimental condition and/or the study hypothesis during data collection.*
Timing	*Indicate the start and stop dates of data collection. If there is a gap between collection periods, state the dates for each sample cohort.*
Data exclusions	*If no data were excluded from the analyses, state so OR if data were excluded, provide the exact number of exclusions and the rationale behind them, indicating whether exclusion criteria were pre-established.*
Non-participation	*State how many participants dropped out/declined participation and the reason(s) given OR provide response rate OR state that no participants dropped out/declined participation.*
Randomization	*If participants were not allocated into experimental groups, state so OR describe how participants were allocated to groups, and if allocation was not random, describe how covariates were controlled.*

Ecological, evolutionary & environmental sciences study design

All studies must disclose on these points even when the disclosure is negative.

Study description	*Briefly describe the study. For quantitative data include treatment factors and interactions, design structure (e.g. factorial, nested, hierarchical), nature and number of experimental units and replicates.*
Research sample	*Describe the research sample (e.g. a group of tagged Passer domesticus, all Stenocereus thurberi within Organ Pipe Cactus National Monument), and provide a rationale for the sample choice. When relevant, describe the organism taxa, source, sex, age range and any manipulations. State what population the sample is meant to represent when applicable. For studies involving existing datasets, describe the data and its source.*
Sampling strategy	*Note the sampling procedure. Describe the statistical methods that were used to predetermine sample size OR if no sample-size calculation was performed, describe how sample sizes were chosen and provide a rationale for why these sample sizes are sufficient.*
Data collection	*Describe the data collection procedure, including who recorded the data and how.*
Timing and spatial scale	*Indicate the start and stop dates of data collection, noting the frequency and periodicity of sampling and providing a rationale for these choices. If there is a gap between collection periods, state the dates for each sample cohort. Specify the spatial scale from which the data are taken*
Data exclusions	*If no data were excluded from the analyses, state so OR if data were excluded, describe the exclusions and the rationale behind them, indicating whether exclusion criteria were pre-established.*
Reproducibility	*Describe the measures taken to verify the reproducibility of experimental findings. For each experiment, note whether any attempts to repeat the experiment failed OR state that all attempts to repeat the experiment were successful.*
Randomization	*Describe how samples/organisms/participants were allocated into groups. If allocation was not random, describe how covariates were controlled. If this is not relevant to your study, explain why.*
Blinding	*Describe the extent of blinding used during data acquisition and analysis. If blinding was not possible, describe why OR explain why blinding was not relevant to your study.*

Did the study involve field work? ☐ Yes ☐ No

Field work, collection and transport

Field conditions	*Describe the study conditions for field work, providing relevant parameters (e.g. temperature, rainfall).*
Location	*State the location of the sampling or experiment, providing relevant parameters (e.g. latitude and longitude, elevation, water depth).*
Access & import/export	*Describe the efforts you have made to access habitats and to collect and import/export your samples in a responsible manner and in compliance with local, national and international laws, noting any permits that were obtained (give the name of the issuing authority, the date of issue, and any identifying information).*
Disturbance	*Describe any disturbance caused by the study and how it was minimized.*

Reporting for specific materials, systems and methods

We require information from authors about some types of materials, experimental systems and methods used in many studies. Here, indicate whether each material, system or method listed is relevant to your study. If you are not sure if a list item applies to your research, read the appropriate section before selecting a response.

Materials & experimental systems

n/a	Involved in the study
☐	☒ Antibodies
☐	☐ Eukaryotic cell lines
☐	☐ Palaeontology and archaeology
☐	☒ Animals and other organisms
☐	☐ Clinical data
☐	☐ Dual use research of concern
☐	☐ Plants

Methods

n/a	Involved in the study
☐	☐ ChIP-seq
☐	☐ Flow cytometry
☐	☐ MRI-based neuroimaging

Antibodies

Antibodies used	None used
Validation	*Describe the validation of each primary antibody for the species and application, noting any validation statements on the manufacturer's website, relevant citations, antibody profiles in online databases, or data provided in the manuscript.*

Eukaryotic cell lines

Policy information about cell lines and Sex and Gender in Research

Cell line source(s)	*State the source of each cell line used and the sex of all primary cell lines and cells derived from human participants or vertebrate models.*
Authentication	*Describe the authentication procedures for each cell line used OR declare that none of the cell lines used were authenticated.*
Mycoplasma contamination	*Confirm that all cell lines tested negative for mycoplasma contamination OR describe the results of the testing for mycoplasma contamination OR declare that the cell lines were not tested for mycoplasma contamination.*
Commonly misidentified lines (See ICLAC register)	*Name any commonly misidentified cell lines used in the study and provide a rationale for their use.*

Palaeontology and Archaeology

Specimen provenance	*Provide provenance information for specimens and describe permits that were obtained for the work (including the name of the issuing authority, the date of issue, and any identifying information). Permits should encompass collection and, where applicable, export.*
Specimen deposition	*Indicate where the specimens have been deposited to permit free access by other researchers.*

Dating methods	*If new dates are provided, describe how they were obtained (e.g. collection, storage, sample pretreatment and measurement), where they were obtained (i.e. lab name), the calibration program and the protocol for quality assurance OR state that no new dates are provided.*

☐ Tick this box to confirm that the raw and calibrated dates are available in the paper or in Supplementary Information.

Ethics oversight	*Identify the organization(s) that approved or provided guidance on the study protocol, OR state that no ethical approval or guidance was required and explain why not.*

Note that full information on the approval of the study protocol must also be provided in the manuscript.

Animals and other research organisms

Policy information about studies involving animals; ARRIVE guidelines recommended for reporting animal research, and Sex and Gender in Research

Laboratory animals	Mice were wild type C57/BL6 (Jackson Laboratories strain 000664), aged 8-45 weeks, of both male and female sex
Wild animals	No wild animals
Reporting on sex	Both male and female mice were used, information preference data are reported disaggregated, and no difference was observed.
Field-collected samples	N/A
Ethics oversight	All experimental and surgical protocols were performed in accordance with the guide of Care and Use of Laboratory Animals (NIH) and were approved by the Institutional Animal Care and Use Committee at Columbia University.

Note that full information on the approval of the study protocol must also be provided in the manuscript.

Clinical data

Policy information about clinical studies

All manuscripts should comply with the ICMJE guidelines for publication of clinical research and a completed CONSORT checklist must be included with all submissions.

Clinical trial registration	*Provide the trial registration number from ClinicalTrials.gov or an equivalent agency.*
Study protocol	*Note where the full trial protocol can be accessed OR if not available, explain why.*
Data collection	*Describe the settings and locales of data collection, noting the time periods of recruitment and data collection.*
Outcomes	*Describe how you pre-defined primary and secondary outcome measures and how you assessed these measures.*

Dual use research of concern

Policy information about dual use research of concern

Hazards

Could the accidental, deliberate or reckless misuse of agents or technologies generated in the work, or the application of information presented in the manuscript, pose a threat to:

No	Yes	
☒	☐	Public health
☒	☐	National security
☒	☐	Crops and/or livestock
☒	☐	Ecosystems
☒	☐	Any other significant area

Experiments of concern

Does the work involve any of these experiments of concern:

No	Yes	
☒	☐	Demonstrate how to render a vaccine ineffective
☒	☐	Confer resistance to therapeutically useful antibiotics or antiviral agents
☒	☐	Enhance the virulence of a pathogen or render a nonpathogen virulent
☒	☐	Increase transmissibility of a pathogen
☒	☐	Alter the host range of a pathogen
☒	☐	Enable evasion of diagnostic/detection modalities
☒	☐	Enable the weaponization of a biological agent or toxin
☒	☐	Any other potentially harmful combination of experiments and agents

Plants

Seed stocks

Report on the source of all seed stocks or other plant material used. If applicable, state the seed stock centre and catalogue number. If plant specimens were collected from the field, describe the collection location, date and sampling procedures.

Novel plant genotypes

Describe the methods by which all novel plant genotypes were produced. This includes those generated by transgenic approaches, gene editing, chemical/radiation-based mutagenesis and hybridization. For transgenic lines, describe the transformation method, the number of independent lines analyzed and the generation upon which experiments were performed. For gene-edited lines, describe the editor used, the endogenous sequence targeted for editing, the targeting guide RNA sequence (if applicable) and how the editor was applied.

Authentication

Describe any authentication procedures for each seed stock used or novel genotype generated. Describe any experiments used to assess the effect of a mutation and, where applicable, how potential secondary effects (e.g. second site T-DNA insertions, mosiacism, off-target gene editing) were examined.

ChIP-seq

Data deposition

☐ Confirm that both raw and final processed data have been deposited in a public database such as GEO.

☐ Confirm that you have deposited or provided access to graph files (e.g. BED files) for the called peaks.

Data access links
May remain private before publication.

For "Initial submission" or "Revised version" documents, provide reviewer access links. For your "Final submission" document, provide a link to the deposited data.

Files in database submission

Provide a list of all files available in the database submission.

Genome browser session
(e.g. UCSC)

Provide a link to an anonymized genome browser session for "Initial submission" and "Revised version" documents only, to enable peer review. Write "no longer applicable" for "Final submission" documents.

Methodology

Replicates

Describe the experimental replicates, specifying number, type and replicate agreement.

Sequencing depth

Describe the sequencing depth for each experiment, providing the total number of reads, uniquely mapped reads, length of reads and whether they were paired- or single-end.

Antibodies

Describe the antibodies used for the ChIP-seq experiments; as applicable, provide supplier name, catalog number, clone name, and lot number.

Peak calling parameters

Specify the command line program and parameters used for read mapping and peak calling, including the ChIP, control and index files used.

Data quality

Describe the methods used to ensure data quality in full detail, including how many peaks are at FDR 5% and above 5-fold enrichment.

Software

Describe the software used to collect and analyze the ChIP-seq data. For custom code that has been deposited into a community repository, provide accession details.

Flow Cytometry

Plots

Confirm that:

☐ The axis labels state the marker and fluorochrome used (e.g. CD4-FITC).

☐ The axis scales are clearly visible. Include numbers along axes only for bottom left plot of group (a 'group' is an analysis of identical markers).

☐ All plots are contour plots with outliers or pseudocolor plots.

☐ A numerical value for number of cells or percentage (with statistics) is provided.

Methodology

Sample preparation	*Describe the sample preparation, detailing the biological source of the cells and any tissue processing steps used.*
Instrument	*Identify the instrument used for data collection, specifying make and model number.*
Software	*Describe the software used to collect and analyze the flow cytometry data. For custom code that has been deposited into a community repository, provide accession details.*
Cell population abundance	*Describe the abundance of the relevant cell populations within post-sort fractions, providing details on the purity of the samples and how it was determined.*
Gating strategy	*Describe the gating strategy used for all relevant experiments, specifying the preliminary FSC/SSC gates of the starting cell population, indicating where boundaries between "positive" and "negative" staining cell populations are defined.*

☐ Tick this box to confirm that a figure exemplifying the gating strategy is provided in the Supplementary Information.

Magnetic resonance imaging

Experimental design

Design type	*Indicate task or resting state; event-related or block design.*
Design specifications	*Specify the number of blocks, trials or experimental units per session and/or subject, and specify the length of each trial or block (if trials are blocked) and interval between trials.*
Behavioral performance measures	*State number and/or type of variables recorded (e.g. correct button press, response time) and what statistics were used to establish that the subjects were performing the task as expected (e.g. mean, range, and/or standard deviation across subjects).*

Acquisition

Imaging type(s)	*Specify: functional, structural, diffusion, perfusion.*
Field strength	*Specify in Tesla*
Sequence & imaging parameters	*Specify the pulse sequence type (gradient echo, spin echo, etc.), imaging type (EPI, spiral, etc.), field of view, matrix size, slice thickness, orientation and TE/TR/flip angle.*
Area of acquisition	*State whether a whole brain scan was used OR define the area of acquisition, describing how the region was determined.*

Diffusion MRI ☐ Used ☐ Not used

Preprocessing

Preprocessing software	*Provide detail on software version and revision number and on specific parameters (model/functions, brain extraction, segmentation, smoothing kernel size, etc.).*
Normalization	*If data were normalized/standardized, describe the approach(es): specify linear or non-linear and define image types used for transformation OR indicate that data were not normalized and explain rationale for lack of normalization.*
Normalization template	*Describe the template used for normalization/transformation, specifying subject space or group standardized space (e.g. original Talairach, MNI305, ICBM152) OR indicate that the data were not normalized.*
Noise and artifact removal	*Describe your procedure(s) for artifact and structured noise removal, specifying motion parameters, tissue signals and physiological signals (heart rate, respiration).*

Volume censoring

Define your software and/or method and criteria for volume censoring, and state the extent of such censoring.

Statistical modeling & inference

Model type and settings

Specify type (mass univariate, multivariate, RSA, predictive, etc.) and describe essential details of the model at the first and second levels (e.g. fixed, random or mixed effects; drift or auto-correlation).

Effect(s) tested

Define precise effect in terms of the task or stimulus conditions instead of psychological concepts and indicate whether ANOVA or factorial designs were used.

Specify type of analysis: ☐ Whole brain ☐ ROI-based ☐ Both

Statistic type for inference

Specify voxel-wise or cluster-wise and report all relevant parameters for cluster-wise methods.

(See Eklund et al. 2016)

Correction

Describe the type of correction and how it is obtained for multiple comparisons (e.g. FWE, FDR, permutation or Monte Carlo).

Models & analysis

n/a	Involved in the study
☐	☐ Functional and/or effective connectivity
☐	☐ Graph analysis
☐	☐ Multivariate modeling or predictive analysis

Functional and/or effective connectivity

Report the measures of dependence used and the model details (e.g. Pearson correlation, partial correlation, mutual information).

Graph analysis

Report the dependent variable and connectivity measure, specifying weighted graph or binarized graph, subject- or group-level, and the global and/or node summaries used (e.g. clustering coefficient, efficiency, etc.).

Multivariate modeling and predictive analysis

Specify independent variables, features extraction and dimension reduction, model, training and evaluation metrics.